AAC Accepted Manuscript Posted Online 1 June 2015
Antimicrob. Agents Chemother. doi:10.1128/AAC.00098-15

Green synthesis of silver and titanium dioxide nanoparticles using *Euphorbia prostrata* extract showed shift from apoptosis to G0/G1 arrest followed by necrotic cell death in *Leishmania donovani*

Abdul Abduz Zahir[1**], Indira Singh Chauhan[2**], Asokan Bagavan[1], Chinnaperumal Kamaraj[1], Gandhi Elango[1], Jai Shankar[4], Nidhi Arjaria[4], Selvaraj Mohana Roopan[3], Abdul Abdul Rahuman[1#] and Neeloo Singh[2#]

[1]*Unit of Nanotechnology and Bioactive Natural Products, Post Graduate and Research Department of Zoology, C. Abdul Hakeem College, Melvisharam-632509, Vellore District, Tamil Nadu, India*

[2]*Biochemistry Division, CSIR Central Drug Research Institute, Jankipuram Extension, Sitapur Road, Lucknow- 226031, India*

[3]*Organic & Medicinal Chemistry Research Laboratory, Organic Chemistry Division, School of Advanced Sciences, VIT University, Vellore-632 014, Tamil Nadu, India*

[4]*Transmission Electron Microscopy, CSIR Indian Institute of Toxicology Research, M.G. Marg Lucknow-226001, India*

Running title: Antileishmanial Nano Compounds

**Contributed equally as joint first authors

[#] *To whom correspondence should be addressed: E-mail*: neeloo888@yahoo.com, abdulrahuman6@hotmail.com

Abstract

The aim of the present study is to synthesize silver (Ag) and titanium dioxide (TiO_2) nanoparticles (NPs) using green synthesis from aqueous leaves extract of *Euphorbia prostrata* as antileishmanial agents and to explore the underlying molecular mechanism of induced cell death. *In vitro* antileishmanial activity of synthesized NPs was tested against promastigotes of *Leishmania donovani* by alamarBlue® and propidium iodide uptake assay. Antileishmanial activity of synthesized NPs on intracellular amastigotes was assessed by Giemsa staining. The leishmanicidal effect of synthesized Ag NPs was further confirmed by DNA fragmentation assay; cell cycle progression and transmission electron microscopy (TEM) of the treated parasites. TEM analysis of the synthesized Ag NPs showed spherical shape with an average size of 12.82 ± 2.50 nm and in comparison to synthesized TiO_2 NPs, synthesized Ag NPs were found to be most active against *Leishmania* parasites after 24 h exposure with IC_{50} value of 14.94 µg/ml and 3.89 µg/ml in promastigotes and intracellular amastigotes respectively. A significant increase in G0/G1 phase of the cell cycle with subsequent decrease in S (synthesis) and G2/M phases when compared to control was observed. The growth inhibitory effect of synthesized Ag NPs was attributed to increased length of S phase. Decreased reactive oxygen species level was also observed which could be responsible for caspase independent shift from apoptosis (G0/G1 arrest) to massive necrosis. High molecular weight DNA fragmentation as a positive consequence of necrotic cell death was also visualized. We also report that the unique trypanothione/trypanothione reductase (TR) system of *Leishmania* cells was significantly inhibited by synthesized Ag NPs. The green synthesized Ag NPs may provide promising leads

46 for the development of cost effective and safer alternative treatment against visceral
47 leishmaniasis.
48
49 **Introduction**
50
51 Neglected diseases caused by parasites are the second leading cause of mortality and
52 impose a substantial burden of morbidity round the globe and more predominantly in the
53 developing countries. Leishmaniasis currently threatens 350 million people in 88 countries
54 around the world. Two million new cases are considered to occur annually, with an estimated 12
55 million people presently infected (1). Among different leishmanial infections, visceral
56 leishmaniasis (VL) caused by *Leishmania donovani* is the most threatening parasite. Although
57 miltefosine and amphotericin B are used for clinical treatment, the antileishmanial drug arsenal
58 still requires improvement (2). For instance, miltefosine monotherapy has failed to cure relapsing
59 VL in HIV-infected patients and thus its role against the HIV-associated VL remains unclear (3).
60 Nanomedicine is defining the use of nanotechnology in medicine, which has been of
61 great interest in recent years. The use of nanoparticles (NPs) for therapeutics is one of the
62 purposes of nanomedicine (4, 5). In recent years, an increasing percentage of nanomaterials are
63 emerging and making advancement in different fields. NPs play an indispensable role in drug
64 delivery, diagnostics, imaging, sensing, gene delivery, artificial implants and tissue engineering
65 (6). Sinha et al. (7) have reported that the biosynthesis of NPs is advantageous over chemical and
66 physical methods as it is a cost-effective and environment friendly method, where it is not
67 necessary to use high pressure, energy, temperature and toxic chemicals. Silver nanoparticles
68 (Ag NPs) have several important applications in the field of biolabelling, sensors, antimicrobial

69 agents and filters. They are capable of purifying drinking water, degrading pesticides and killing
70 human pathogenic bacteria (8). Ag NPs have been used in the treatment and improvement of
71 drug delivery against leishmaniasis (9-12). Silver polypyridyl complexes are biologically active
72 against *Leishmania mexicana*, where they interact with DNA (13). Similarly, nano-preparations
73 with titanium dioxide nanoparticles (TiO_2 NPs) are currently under investigation as novel
74 treatments for acne vulgaris, recurrent condyloma accuminata, atopic dermatitis, hyperpigmented
75 skin lesions and other non dermatologic diseases (14). Quercetin (polyphenolic compound)
76 conjugated gold NPs have also been evaluated against promastigotes and amastigotes of *L.*
77 *donovani* (15).

78 There are limited studies concerning the green synthesis of NPs and its control efficacy
79 against *Leishmania* parasites. Among the various biosynthetic approaches, the use of plant
80 extracts is preferable as they are easily available, safe to handle and possess a broad viability of
81 metabolites. The potential of plants as biological materials for the synthesis of NPs is yet to be
82 fully explored (16). *Euphorbia prostrata* is a small, prostrate and hispidly pubescent annual herb
83 found all over India. The leaves extract of *E. prostrata* showed antibacterial, nematicidal and
84 antiparasitic activities (17). Anthraquinones, flavonoids, phenols, phlobotannins,
85 polysaccharides, saponins, tannins and terpenoids were isolated from the leaves extract of *E.*
86 *prostrata* (18). The flavonoids were promising compounds for controlling human and animal
87 parasitic diseases (19). Phenolic compounds were tested against *Leishmania* spp. and for
88 immunomodulatory effects on macrophages (20). Similarly, the antileishmanial activities of
89 terpenoid derivatives were tested against promastigotes and intracellular amastigotes form of *L.*
90 *donovani* (21). In the present study, the antileishmanial activity of green synthesized Ag NPs and

91 TiO_2 NPs using the aqueous leaves extract of *E. prostrata* were evaluated against promastigotes
92 and intracellular amastigotes of *L. donovani*.
93
94 **Methods**
95
96 **Synthesis of Ag NPs and TiO_2 NPs.** Fresh leaves of *E. prostrata* were collected in and
97 around Melvisharam, Vellore district, Tamil Nadu, India. The aqueous leaves extract was
98 prepared by taking 2 g of finely cut leaves in 250 ml of Erlenmeyer flask along with 100 ml of
99 sterilized double distilled water and boiling the mixture at 60°C for 15 – 20 min. The extract was
100 filtered with Whatman filter paper no. 1, stored at −20°C and used within a week. The
101 biosynthesis of Ag NPs was carried out using different compositions of the aqueous leaves
102 extract with $AgNO_3$ solution (3:97, 6:94, 9:91, 12:88 and 15:85 ml). The reaction mixture was
103 periodically observed for the change in color and analyzed by UV-Vis spectrophotometer in the
104 range of 100 - 700 nm. Total volume of 88 ml of 1 mM $AgNO_3$ solution was reduced using 12 ml
105 of aqueous leaves extract of *E. prostrata* at room temperature for 6 h, resulting in a brown
106 yellow colored solution indicating the formation of synthesized Ag NPs (22). For synthesis of
107 TiO_2 NPs, the Erlenmeyer flask containing 100 ml of 5 mM $TiO(OH)_2$ was stirred for 2 h.
108 Different proportions of aqueous leaves extract of *E. prostrata* were prepared and interacted with
109 the $TiO(OH)_2$ solution mixing ratio of 5:95, 10:90, 15:85, 20:80 and 25:75 ml, separately. 20 ml
110 of aqueous leaves extract of *E. prostrata* was added to 80 ml of $TiO(OH)_2$ solution for the
111 optimization of TiO_2 NPs synthesis. The pure $TiO(OH)_2$ solution and the aqueous leaves extract
112 didn't show any color change. Whereas in the leaves extract with $TiO(OH)_2$ showed the change
113 of color to light green. Different reaction parameters (concentrations of plant extract, substrate

114 concentrations, pH, temperature and reaction time) were optimized to synthesize NPs with
115 controlled properties (23).

116 **Characterization of synthesized NPs.** Synthesis of NPs solution with leaves extract was
117 observed by UV–Vis spectroscopy. The bioreduction of ions in the solutions was monitored by
118 periodic sampling of aliquots (1 ml) of the aqueous component after 20 times dilution and
119 measured in the UV–Vis spectra. Samples were monitored as a function of time of reaction using
120 Shimadzu 1601 spectrophotometer in the 100–700 nm range operated at a resolution of 1 nm.
121 The reduced solution centrifuged at 8000 rpm for 40 min and resulting pellet was redispersed in
122 deionized water. Adsorbed substances on the surface of the synthesized NPs were removed by
123 repeated washing.

124 Thus obtained purified and dried pellet of synthesized Ag NPs and TiO_2 NPs were subjected
125 to X-ray diffraction (XRD) analysis. For XRD studies, dried NPs were coated on XRD grid, and
126 the spectra were recorded by using Phillips PW 1830 instrument operating at a voltage of 40 kV
127 and a current of 30 mA with Cu Kα1 radiation. Fourier transform infrared (FTIR) analysis of the
128 samples were carried out using Perkin Elmer spectrophotometer in the diffuse reflectance mode
129 at a resolution of 4 cm^{-1} in KBr pellet and showed possible functional groups for the formation
130 of NPs. Topography of synthesized NPs was studied using AFM analysis (Atomic force
131 microscopy –Veeco Innova, USA). Images have been processed using XEI software given by
132 Park system. The synthesized NPs were examined using Innova advanced scanning probe
133 microscope (CP-II, Veeco Instruments Inc., USA) in a non-contact tapping mode. A thin film of
134 the sample was prepared on a glass slide by dropping 100 µl of the sample on the slide, and
135 allowed to dry for 5 min. Topographical images were obtained in non-contact mode using silicon
136 nitride tips at a resonance frequency of 218 kHz in ambient air by oscillating the cantilever

137 assembly at or near the cantilever's resonant frequency using a piezoelectric crystal.
138 Characterization was done by observing the patterns on the surface topography and data analysis
139 through WSXM software (24). The size of the NPs was confirmed by using TEM analysis
140 (Transmission electron microscopy – Hitachi H-7100) using an accelerating voltage of 120 kV
141 and methanol as solvent.

142 **Gas chromatography-mass spectrometry (GC–MS) analysis.** The chemical
143 composition of aqueous leaves extract of *E. prostrata* was analyzed using GC–MS (GCD-
144 HP1800A system, Hewlett-Packard, USA) equipped with a split/split less capillary injection
145 port. For GC–MS detection, an electron ionization system (quadruples analyzer; mass range, 10–
146 425 amu) with ionization energy of 70 eV was used. Each of these steps carried out under high
147 vacuum from 10^{-4} to 10^{-8} torr. Helium gas was used as a carrier at a constant flow rate of 1
148 ml/min. Injector and mass transfer line temperatures were set at 250°C and 280°C, respectively.
149 The components of aqueous leaves extract of *E. prostrata* were identified after comparison with
150 the available data in library (NIST) attached to the GC–MS instrument and reported (25).

151 **Macrophage culture.** The J774A.1 mouse (BALB/c) macrophage cell line was obtained
152 from National Centre for Cell Science (Pune, India) and used as a cellular host for the *in*
153 *vitro* intracellular test of antileishmanial activity against amastigotes. The cells were maintained
154 in RPMI 1640 medium (Gibco-BRL) adjusted to contain 2 g of sodium bicarbonate/liter, 6 g of
155 HEPES/liter, 10% (v/v) heat-inactivated fetal bovine serum (HI-FBS; Gibco, Germany), and 100
156 U penicillin and 100 µg of streptomycin/ml at 37°C in a humidified atmosphere of 95% air and
157 5% CO_2 (26).

158 **Parasite culture and analysis of cell viability.** Promastigotes of *L. donovani* strain
159 (MHOM/IN/80/DD8) were routinely cultured as described previously (27). AlamarBlue® cell

160 viability reagent (Invitrogen, Cat. No. DAL1025, Carisbad, CA) was used for evaluation of
161 antileishmanial activity of synthesized Ag NPs. Logarithmic phase promastigotes of *L. donovani*
162 (50,000 cells, final volume 200 µl/well) were seeded in 96 well microtiter plates (Greiner, bio-
163 one, Germany) in the presence of different concentrations (0, 12.5, 25, 50 and 100 µg/ml) of
164 synthesized Ag NPs and incubated at 25°C for 24 h. Miltefosine was used as the standard drug.
165 20 µl of AlamarBlue® was added to each well and the plate was further incubated at 25°C for 4
166 h. Absorbance was measured in a ELISA reader (Biotek Instruments, Epoch) using λ=570 nm as
167 test wavelength (resorufin) and λ=600 nm as reference wavelength (resazurin) serving as blank.
168 The oxidized form of AlamarBlue® resazurin (non toxic, cell permeable and blue in colour) was
169 reduced by metabolically active cells to resorufin (highly fluorescent, red in colour). Percentage
170 of cell viability of promastigotes treated with synthesized Ag NPs was analyzed by the following
171 formula (28).

172 Percentage of cell viability = Untreated control λ (570 – 600 nm) – treated set λ (570 –
173 600 nm) / untreated control λ (570 – 600 nm) X 100.

174 ***In vitro* evaluation of antileishmanial activity of synthesized Ag NPs in intracellular**
175 **amastigotes**. The J774A.1, mouse (BALB/c) macrophages cell line, 4000 cells per well, final
176 volume 200 µl of RPMI-1640 medium were seeded in 8 well chamber slide (Nunc™ Lab-Tek™
177 II Chamber Slide™ System). The cells were allowed to adhere for 8 h at 37°C in carbon dioxide
178 incubator with 5% CO2. Non adherent cells were removed and these cells were infected with
179 stationary phase promastigotes of *L. donovani* in a ratio of 6:1 (parasites/macrophages) and
180 incubated at 37°C in 5% CO_2 for 0- 18 h. At 18 h after the parasites entered macrophages, free
181 parasites were eliminated and infected macrophages were treated with increasing concentrations
182 (0, 2.5, 5 and 10 µg/ml) of synthesized Ag NPs, incubated at 37°C in 5% CO_2 for 24 h. After

183 indicated incubation time, infected macrophages treated with or without synthesized Ag NPs, in
184 chamber slides were fixed with ice-cold methanol and slides were then submerged in 10% (v/v)
185 Giemsa staining solution (Thomas Baker) for 45 min, briefly washed in water and set to dry. The
186 slides were viewed on an inverted bright field microscope (IX73 Inverted Microscope, Olympus)
187 (29). At least 100 macrophages per well from duplicate cultures were counted to calculate the
188 percentage of infected macrophages using this formula (30).

189 % Reduction = Number of amastigotes per 100 macrophages (treated samples) / number
190 of amastigotes per 100 macrophages (infected control) X 100.

191 IC_{50}, the concentration of drug that is cytotoxic to 50% of the amastigotes, was obtained by
192 plotting the graph of percentage of cell viability versus different concentrations of synthesized
193 Ag NPs.

194 ***In vitro* cytotoxicity in macrophages.** The J774A.1 cells were incubated in a 96-well
195 plate containing 50,000 cells/well. The plates were incubated overnight in a CO_2 incubator, with
196 a supply of 5% CO_2 at 37°C. The synthesized Ag NPs, at different concentrations (0, 5, 10 and
197 20 µg/ml) was dispensed in triplicate, and three wells were left as control wells. The plates were
198 incubated for 24 h, and MTT [3-(4,5-dimethylthiazole-2-yl)-2-5-diphenyl tetrazolium bromide]
199 assay was performed to assess cell proliferation or viability (27). The 50% cytotoxic
200 concentration (CC_{50}) was determined by logarithmic regression analysis using GraphPrism 5
201 software.

202 **Transmission electron microscopy.** TEM analysis was carried out to observe the
203 ultrastructural changes in the morphology of *L. donovani* promastigotes induced by synthesized
204 Ag NPs. Parasites were incubated in the presence of synthesized Ag NPs at IC_{50} dose for 45 min,
205 washed with PBS (pH 7.2) prior to fixing in 2.5% glutraldehyde in sodium cacodylate (Ladd

206 Research Industries, USA) buffer (pH 7.2) for 2 h at 4°C. Fixed parasites were centrifuged at
207 3500 x g for 10 min and washed 3 times with 0.1 M sodium cacodylate buffer and post fixed in
208 1% osmium tetraoxide for 2 h. Post fixed parasites were washed with sodium cacodylate and
209 dehydrated in ascending acetone series (15, 30, 60 and 100%), embedded in araldite-DDSA
210 mixture (Ladd Research Industries, USA) and baked at 60°C for 48 h. After baking, blocks were
211 cut (60-80 nm thick) by an ultramicrotome (Leica EM UC7, Vienna, Austria), mounted on
212 copper grids and double stained with uranyl acetate and lead citrate. Analysis of stained sections
213 were examined by TEM (TECNAI G2 SPIRIT, FEI, Netherland) equipped with Gatan Orius
214 camera at 80 KV (31).

215 **Propidium iodide uptake assay.** Logarithmic phase promastigotes of *L. donovani*
216 (1×10^6 cells, final volume 2 ml/well) were seeded in 6 well microtiter plates (Greiner, bio-one,
217 Germany) in the presence of different concentrations (12.5, 25 and 50 µg/ml) of synthesized Ag
218 NPs and incubated at 25°C for 24 h. After indicated incubation times, cells were centrifuged
219 (3500 x g for 10 min), washed once with PBS (pH 7.2), resuspended in 50 µg/ml final
220 concentration of propidium iodide (PI) (Sigma-Aldrich, Cat. No. SLBF5585V, St. Louis, MO,
221 USA), and incubated for 30 min in the dark at room temperature. Unbound PI was removed by
222 washing and samples were processed on a FACS Calibur flow cytometer (BD Bioscience, San
223 Jose, CA, USA). Fluorescence of the propidium iodide (PI) was collected in the FL2 channel,
224 equipped with a 585/42 nm band pass filter. Analysis for mean fluorescence intensity was done
225 using CellQuest Pro software (BD Biosciences, CA). 20,000 events from each sample were
226 acquired to ensure adequate data and the histogram and images are representative of three
227 independent experiments (32, 33).

228 **Analysis of externalized phosphatidylserine.** To quantify the percentage of parasites
229 undergoing apoptosis, annexin-V-FITC and PI dual staining was performed as per the
230 manufacturer's instructions (AnnexinV-FITC Apoptosis detection kit, Sigma, MO, USA). In
231 brief 2×10^6 cells/ml log phase *L. donovani* promastigotes were treated with different
232 concentrations (12.5, 25 and 50 µg/ml) of synthesized Ag NPs for 24 h and cells were
233 centrifuged (3500 x g for 5 min), washed twice in PBS and resuspended in annexin V binding
234 buffer [10 mM Hepes/NaOH (pH 7.4), 140 mM NaCl and 2.5 mM $CaCl_2$]. Annexin V-FITC and
235 PI were then added according to the manufacturer's instructions and incubated for 15 min in the
236 dark at 20–25°C. The percentages of viable and dead cells were determined from 10,000 cells
237 per sample, by using the FL1 channel for annexin V and the FL2 channel for PI on FACS
238 Calibur flow cytometer (BD Bioscience, San Jose, CA, USA). The histogram and images are
239 representative of three independent experiments (34).

240 **Cell cycle analysis.** Briefly 2×10^6 cells/ml log phase *L. donovani* promastigotes were
241 treated with different concentrations (12.5, 25 and 50 µg/ml) of synthesized Ag NPs for 24 h and
242 were harvested by centrifugation at 3500 x g for 5 min at 4°C. Cells were washed once in 1 ml
243 PBS and then fixed by incubation in 70% ethanol: 30% PBS for 1 h at 4°C. Fixed cells were
244 harvested by centrifugation at 1750 x g for 10 min at 4°C, washed in 1 ml PBS and resuspended
245 in 1 ml PBS with RNAse A (100 µg/ml, Fermentas, Cat. No. EN0531) and PI (10 µg/ml). The
246 cells were incubated at room temperature for 45 min and then analysed using FACS Calibur flow
247 cytometer (BD Bioscience, San Jose, CA, USA). Cell cycle distribution was modeled using
248 ModFit LT for Mac V3.0 and 10,000 events from each sample were acquired to ensure adequate
249 data (34). The histogram and images are representative of three independent experiments.

250 **DNA fragmentation assay.** Qualitative analysis of fragmentation was performed by
251 agarose gel electrophoresis of total genomic DNA of treated and untreated parasites (34). Total
252 cellular DNA from promastigotes exposed to different concentrations (12.5, 25 and 50 µg/ml) of
253 synthesized Ag NPs was isolated according to manufacturer`s instructions (Apoptotic DNA
254 ladder detection kit, Cat. No. KHO1021, Molecular Probes, USA). The isolated DNA was
255 quantified spectrophotometrically by the absorbance ratio of 260/280 nm and DNA (1 µg/lane)
256 was separated on 1.2% agarose gel containing ethidium bromide in TBE buffer (50 mM; pH 8.0)
257 for 1.5 h at 75 V, visualized under UV light and photographed using a gel documentation system
258 (Genei™, Uvitech, Cambridge).

259 **Terminal deoxynucleotidyl transferase-mediated dUTP nick-end labelling (TUNEL)**
260 **assay.** Fragmentation of DNA into nucleosomal bands, as a function of apoptotic cell death was
261 studied by DNA laddering assay. DNA fragmentation within the cell can be analyzed by
262 Terminal Deoxynucleotidyltranferase (TdT)-mediated dUTP Nick End Labeling (TUNEL) using
263 an APO-BRDU (a flow cytometry kit for apoptosis, Sigma) assay kit according to the
264 manufacturer's instructions. The TUNEL technique is able to quantify the proportion of DNA
265 fragments by binding to BrdU via TdT. Thus, the amount of DNA fragments is directly
266 proportional to the fluorescence obtained by BrdU incorporation and labeling by anti-BrdU
267 antibody conjugated to FITC. Briefly, promastigotes were incubated with different
268 concentrations (12.5, 25 and 50 µg/ml) of synthesized Ag NPs for 24 h, washed twice in PBS
269 (pH 7.2) and fixed in 1% paraformaldehyde for 15 min. The cells were washed again in PBS and
270 incubated in ice-cold 70% (v/v) ethanol for 30 min in a −20°C freezer. After centrifugation the
271 cells were allowed to react with TdT enzyme in DNA-labeling solution for 60 min at 37°C. The
272 samples were incubated with antibody staining solution containing the FITC–labeled anti-BrdU

273 antibody. Finally, the cells were counterstained with propidium iodide and fluorescence acquired
274 by FACS Calibur flow cytometer (BD Bioscience, San Jose, CA, USA) through dual pass
275 FITC/PI filter set**.** Two dual parameter and two single parameters displays were created with the
276 flow cytometer data acquisition software (CellQuest Pro software, BD Biosciences, CA). The
277 gating display was the standard dual parameter DNA doublet discrimination display with the
278 DNA Area signal on the y-axis and the DNA width on the x-axis. From the above display, a gate
279 was drawn around the non -clumped cells and the second gated dual parameter display was
280 generated. The DNA (Linear Red Fluorescence) was displayed on the x-axis and the Anti-BrdU-
281 FITC (Log Green Fluorescence) on the y-axis. Two single parameters gated histograms, DNA
282 and FITC-BrdU were also be added to determine apoptotic cells and their cell- cycle stages. The
283 histogram and images are representative of three independent experiments. 10,000 events from
284 each sample were acquired to ensure adequate data (35).

285 **Measurement of reactive oxygen species (ROS) level.** Intracellular ROS level was
286 measured in *L. donovani* promastigotes as described previously (36). Briefly, 2×10^6 cells/ml log
287 phase *L. donovani* promastigotes treated with different concentrations of synthesized Ag NPs
288 (12.5, 25 and 50 µg/ml) for 24 h, were washed and resuspended in 500 µl of medium M-199 and
289 loaded with the cell permeant probe 2,7-dichlorodihydrofluorescein diacetate (H_2DCFDA,
290 Sigma) (10 µM) for 30 min at 20-25°C, and fluorescence was monitored. The fluorescent probe
291 H_2DCFDA is one of the most widely used techniques for direct measuring of the redox state of a
292 cell. It is a cell permeable and relatively non-fluorescent molecule. It is also extremely sensitive
293 to the changes in the redox state of a cell and can be used to follow the changes of ROS over
294 time. Activity of cellular esterases cleaves H_2DCFDA into 2,7-dichlorodihydrofluorescein
295 ($DCFH_2$). Peroxidases, cytochrome c and Fe^{2+} can all oxidize $DCFH_2$ to 2,7-dichlorofluorescein

296 (DCF) in the presence of hydrogen peroxide. Accumulation of DCF in the cells was measured by
297 an increase in fluorescence at 530 nm when the sample was excited at 485 nm. It is assumed to
298 be proportional to the concentration of hydrogen peroxide in the cells (34). Fluorescence of the
299 2,7-dichlorofluorescein (DCF) was collected in the FL1 channel, equipped with a 530/30 nm
300 band pass filter on FACS Calibur flow cytometer (BD Bioscience). Fluorescence was measured
301 in the log mode using CellQuest Pro software (BD Biosciences, CA) and expressed as mean
302 fluorescence intensity. 10,000 events from each sample were acquired to ensure adequate data.
303 The histogram and images are representative of three independent experiments.

304 **Measurement of intracellular non-protein thiols.** 5-chloromethylfluorescein-diacetate
305 (CMFH-DA, cellTracker™ Green CMFDA, Cat.No.C7025, Molecular Probes, USA) is a cell
306 permeable, non-fluorescent dye that upon entering into the cell, rapidly binds with non-protein
307 thiols and becomes non-permeable; the simultaneous cleavage of the diacetate moiety by cellular
308 esterases yields a fluorescent thioether. Accordingly, the detected fluorescence is directly
309 proportional to the amount of intracellular non-protein thiols (37). 2×10^6 cells/ml log phase of *L.*
310 *donovani* promastigotes treated with aqueous leaves extract of *E. prostrata*, synthesized Ag NPs
311 and $AgNO_3$ solution for 24 h, were collected into 1.5 ml micro centrifuge tubes and centrifuged
312 at 1000 x g for 5 min to remove the supernatant. Then the cell pellets were washed with PBS,
313 incubated with 5-chloromethylfluorescein-diacetate in the dark for 15 min at 37°C and analyzed
314 for fluorescence in the FL1 channel, equipped with a 530/30 nm band pass filter on FACS
315 Calibur flow cytometer (BD Bioscience) and analysis for mean fluorescence intensity was done
316 using CellQuest Pro software. 40,000 events from each sample were acquired to ensure adequate
317 data. The histogram and images are representative of three independent experiments.

Antimicrobial Agents and Chemotherapy

318 **Statistical analysis.** Each experiment was performed at least three times. The data has
319 been summarized in mean ± SD. The comparison of group has been done by one way analysis of
320 variance using GraphPad Prism software. The groups are compared by Dunnett's test after one
321 way annova. The individual comparison has been done New man/Keuls test. p=0.05 has been
322 considered as the level of significance.

323 **Results**

324

325 The leaves extract of *E. prostrata* was mixed in the aqueous solution of the silver ion
326 complex and it started to change the color from watery to brown due to reduction of silver ion
327 which indicated the formation of Ag NPs. NPs formation was monitored by colour change,
328 despite the fact that colour change has been reported to be the initial evidence of NPs formation
329 (23). Results of the present study revealed that the overall optimized reaction conditions for the
330 synthesis of Ag NPs were: concentration of aqueous leaves extract = 12 ml, concentration of
331 $AgNO_3$ solution = 88 ml of 1 mM, temperature = 45°C, pH = 9.0, time = 6 h and the maximum
332 absorption peaks observed at 420 nm. Similarly, synthesized TiO_2 NPs were: concentration of
333 aqueous leaves extract = 20 ml, concentration of $TiO(OH)_2$ solution = 80 ml of 5 mM,
334 temperature = 40°C, pH = 8.0, time = 10 h and the maximum absorption peak observed at 305
335 nm. These results are in good agreement with the previous authors report (23).

336 **Characterization of the synthesized NPs.** The synthesized Ag NPs using *E. prostrata*
337 leaves extract was supported by X-ray diffraction measurements. XRD spectrum was compared
338 with the standard confirmed spectrum of Ag particles formed in the present experiments, which
339 were in the form of nanocrystals, as evidenced by the peaks at 2θ values of 38.26°, 44.45°, 64.58°
340 and 77.49° which were indexed to the planes 111, 200, 220 and 311, respectively. The average

341 grain size of Ag NPs formed in the biosynthesis was determined to be 12.82 ± 2.50 nm for the
342 higher intense peak using Scherrer's formula, $d = 0.89\lambda/\beta \cos\theta$. XRD analysis for the
343 synthesized TiO_2 NPs showed distinct diffraction peaks at 27.63°, 36.27°, 41.43°, 54.49°, 56.80°
344 and 69.16° indexed to the planes 110, 101, 111, 211, 220 and 301, respectively (Fig. 1A). The
345 average grain size of TiO_2 NPs formed in the biosynthesis was determined to be 83.22 ± 1.50
346 nm. The sharp peaks and absence of unidentified peaks confirmed the crystallinity and higher
347 purity of prepared NPs. Dubey et al. (38) reported that the size of nano silver as estimated from
348 the full width at half maximum of the (111) peak of silver using the Scherrer`s formula was 20 –
349 80 nm. XRD peaks at 2θ value of 25.25° (101) confirm the characteristic facets for anatase form
350 of TiO_2 (39). This estimation confirmed the hypothesis of particle monocrystallinity. The
351 sharpening of the peaks clearly indicates that the particles were in the nanoregime.

352 The FTIR spectroscopy is used to probe the chemical composition of the surface and capping
353 agents for the synthesis of NPs. FTIR analysis of synthesized Ag NPs and TiO_2 NPs using the
354 aqueous leaves extract of *E. prostrata* are shown in (Fig. 1B). The synthesized Ag NPs showed
355 the presence of bands due to heterocyclic amine, NH stretch (3431 cm^{-1}), methylene C-H bend
356 (1616 cm^{-1}), gem-dimethyl (1381 cm^{-1}), cyclohexane ring vibrations (1045 cm^{-1}), skeletal C-C
357 vibrations (818 cm^{-1}) and aliphatic iodo compounds, C-I stretch (509 cm^{-1}). The functional
358 groups for *E. prostrata* leaves aqueous extract and synthesized Ag NPs were 548 and 509 cm^{-1}
359 for aliphatic iodo compounds, C-I stretch. Hence, it proves that synthesized Ag NPs have been
360 synthesized with plants compounds involved in the biological reduction of the $AgNO_3$. Similarly,
361 the synthesized TiO_2 NPs showed the presence of bands due to hydroxy group, H-bonded OH
362 stretch (3420 cm^{-1}), methylene C-H asym./sym. stretch (2926 cm^{-1}), secondary amine, NH bend
363 (1618 cm^{-1}), phenol or tertiary alcohol, OH bend (1377 cm^{-1}), cyclic ethers of large rings, C-O

364 stretch (1071 cm^{-1}) and thioethers, CH_3-S-, C-S stretch (649 cm^{-1}). The functional groups of
365 leaves extract and synthesized TiO_2 NPs were 2924 and 2926 cm^{-1} for methylene C-H
366 asym./sym. stretch, 1618 and 1618 cm^{-1} for secondary amine, NH bend. After reduction of
367 $TiO(OH)_2$ the increase in intensity at 2926 cm^{-1} signify the involvement of the around for
368 methylene C-H asym./sym in the reduction process. Hence, it proves that synthesized TiO_2 NPs
369 have been synthesized with *E. prostrata* compounds involved in the biological reduction of the
370 TiO_2 (40).

371 The synthesized NPs were characterized by AFM for its detail size, morphology and
372 agglomeration. Characterization of the synthesized NPs using AFM offered a three-dimensional
373 visualization. The uneven surface morphology was explained by the presence of both individual
374 and agglomerated NPs. The strong crystalline nature was observed in the form of diagonal
375 formations with ridges (Fig. 2 A and B). In accordance with the present results, previous studies
376 have demonstrated that the topographical images of irregular shaped synthesized NPs (41). TEM
377 images of the synthesized Ag NPs and TiO_2 NPs obtained were spherical, quite polydisperse and
378 individual particles showed an average size of 12.82 ± 2.50 and 83.22 ± 1.50 nm, respectively.
379 SAED pattern of the Ag NPs, the ring-like diffraction pattern indicates that the particles were
380 crystalline. The diffraction rings were indexed on the basis of the fcc structure of silver. Four
381 rings arise due to reflections from (111), (200), (220) and (311) lattice planes of fcc silver,
382 respectively. SAED pattern of the TiO_2 NPs, six rings arise due to reflections from (110), (101),
383 (111), (211), (220) and (301) lattice planes of fcc titanium, respectively. This is evident by sharp
384 Braggs reflection observed in the XRD spectrum (Fig. 2 C and D).

385 **GC-MS analysis.** The compounds identified by the GC-MS analysis, the retention time
386 (RT) and percentage peak of the individual compounds in the aqueous leaves extracts of *E.*

387 *prostrata* are shown in Table 1. Four compounds were detected in the aqueous leaves extract, the
388 major chemical constituent was identified as 2,3-dihydrobenzofuran (peak area 27.44%) which
389 could have acted as a reducing and capping agent for the synthesis of Ag NPs and TiO_2 NPs. The
390 other constituents such as 1,3-dihydroisobenzofuran (19.97%), 4-choloro- 2,5-
391 dimethoxybenzamine (21.80%) and methyl 3-(hydroxymethyl) bicycle [3.2.1] oct-6-ene-1-
392 carboxylate (5.53%) were identified.

393 **Analysis of cell viability.** The results showed that the synthesized Ag NPs were most
394 active against promastigotes of *L. donovani* compared to aqueous leaves extract of *E. prostrata*,
395 $AgNO_3$ and $TiO(OH)_2$ solutions and synthesized TiO_2 NPs. Significance level were estimated by
396 one way ANOVA followed by Dunnett`s multiple comparison test and found to be highly
397 significant ($p< 0.001$) for synthesized Ag NPs (Table 2). Decreased mobility of promastigotes
398 treated with aqueous leaves extract of *E. prostrata*, synthesized Ag NPs and $AgNO_3$ solution
399 were observed under light microscope in the first 24 h of treatment. Pronounced morphological
400 changes within the parasite such as round to oval, shape decrease in size with dense cytoplasm
401 and enlarged nuclei were also observed. Soon after 24 h, the morphology of the treated
402 promastigotes was completely destroyed. The IC_{50} values were determined at 24 h of treatment
403 with synthesized Ag NPs. The result showed the IC_{50} log value of 1.17 µg/ml which is equivalent
404 to 14.94 µg/ml in promastigotes (Fig. 3A) and in intracellular amastigotes it showed 0. 58 µg/ml
405 (in log value) which is equivalent to 3.89 µg/ml (Fig. 3B (a)). The antileishmanial activity of
406 synthesized Ag NPs, were also checked against the J774A.1 cell line to determine whether the
407 doses used for IC_{50} determination for intracellular amastigotes were toxic to the cell itself;
408 experiments revealed that the 50% cytotoxic dose (CC_{50}) value was far higher (115.5 µg/ml) than
409 the IC_{50} dose (3.89 µg/ml) for intracellular amastigotes (Fig. 3B (b)).

410 **Transmission electron microscopy.** The TEM study has been the most widely used
411 techniques to visualize agglomerated NPs in cells. The ultrastructural analysis of the
412 promastigotes treated with synthesized Ag NPs showed cytolysis with features of necrosis
413 including a general cell hydration causing swelling of the organelles (endoplasmic reticulum and
414 mitochondria), vacuolization, and gross alterations in the organization of the nuclear and
415 chromatin when compared to control (Fig. 3C).

416 **Propidium iodide uptake assay.** PI uptake was used to quantify the population of cells
417 in which membrane integrity was lost resulting in cell death. Different concentrations of
418 synthesized Ag NPs were used to assess cellular uptake of PI in *L. donovani* promastigotes after
419 24 h treatment. This method has also been applied by other investigators as well (32, 33). Gould
420 et al. (32) have established that propidium-based cell lysis assay a valuable and convenient new
421 method for evaluating the interaction of drug candidates and target cells in culture. The x-axis
422 depicts propidium iodide uptake and the y-axis depicts side scatter (SSC) as shown in (Fig. 4A).
423 Gating was done of the PI negative cells on the basis of them being unscattered as depicted by
424 the y-axis SSC (M1). Hence we are showing increased cell death in the x-axis (M2) by the
425 gradual shifting of the dead cell population (increased MFI) with increased concentration of
426 synthesized Ag NPs. Treated promastigotes undertake PI in a concentration-dependent manner.
427 A sharp increase in PI positive (M2) cells from 19.27 at 12.5 µg/ml to 50.36 at 25 µg/ml and
428 thereafter gradual decrease to 48.01 at 50 µg/ml after 24 h of treatment. Untreated cells which
429 served as control showed no cell death.

430 **Analysis of externalized phosphatidylserine.** To delineate the nature of cell death, *L.*
431 *donovani* promastigotes which were treated with different concentrations (12.5, 25 and 50 µg/ml)
432 of synthesized Ag NPs for 24 h were harvested, washed with PBS and double-stained with

Antimicrobial Agents and Chemotherapy

433 annexin V-FITC and PI. The number of cells that were PI-positive (upper-left quadrant)
434 gradually increased from 34.87, 39.90 and 44.01% at 12.5, 25 and 50 µg/ml, respectively. These
435 observations suggested that synthesized Ag NPs induced cell death by necrosis. The synthesized
436 Ag NPs treated promastigotes showed positive for both annexin V and PI-positive (upper-right
437 quadrant) and decreased in the activity of apoptosis from 13.12 to 6.78% at 12.5 and 50 µg/ml,
438 respectively (Fig. 4B). In contrast, only 0.18% of untreated cells, which served as control were
439 annexin V and PI-positive and showed no cell death. These results are a confirmatory indication
440 of shift from apoptosis to necrosis on treatment of *L. donovani* promastigotes with synthesized
441 Ag NPs.

442 **Cell cycle analysis.** To assess the role of different concentrations (12.5, 25 and 50 µg/ml)
443 of synthesized Ag NPs in mediating G0/G1 arrest and at the end of treatment period (24 h), cell
444 cycle analysis was performed based on PI staining using flow cytometry (42). (Fig. 4C) shows
445 that synthesized Ag NPs (at 12.5 and 25 µg/ml) induced a marked increase in the number of cells
446 in the G0/G1 phase (G1:48.69% versus 60.50% to 62.00%), and simultaneous decrease in both S
447 phase (S: 33.86% versus 31.73% to 27.70%) and G2/M phase compared with control was
448 observed (G2/M: 17.44% versus 7.76% to 10.30%). The concentration-dependent effect on
449 G0/G1 arrest in promastigotes was largely at the expense of S phase cells, with low change in the
450 G2/M-phase cell population compared with the untreated promastigotes. The drug-induced cell
451 cycle perturbations, such as an increase in the number of cells in the G1 phase, have been
452 reported to correlate with a response to chemotherapy (43).

453 **DNA fragmentation assay.** Treatment of promastigotes with different concentrations
454 (12.5, 25 and 50 µg/ml) of synthesized Ag NPs for 24 h and revealed DNA breakage which was

Antimicrobial Agents and Chemotherapy

455 not extensive. High molecular weight DNA fragments ~700 bp were observed (Fig. 4C (f)),
456 which reconfirmed that mode of cell death in promastigotes may be largely due to necrosis.

457 **Terminal deoxynucleotidyl transferase-mediated dUTP nick-end labelling (TUNEL)**
458 **assay.** TUNEL assay was performed in order to verify whether the synthesized Ag NPs was able
459 to induce DNA fragmentation in promastigotes of *L. donovani*. Propidium iodide (total cellular
460 DNA) and fluorescein (Apoptotic Cells) were the two dyes used. Gating (R1) was done within
461 the DNA Area on the y-axis (FL2-A) and the DNA Width on the x-axis (FL2-W) as shown in
462 (Fig. 5A).

463 In (Fig. 5B), **t**he x-axis depicts DNA (propidium iodide, linear red fluorescence and FL2
464 channel) and the y-axis depicts Anti-BrdU-FITC (log green Fluorescence and FL1 channel).
465 Increasing concentrations of synthesized Ag NPs showed the increase number of cells (R2)
466 stained by anti-BrdU which have moved from non apoptotic population (G0/G1 and G2 phase) to
467 the apoptotic population (S phase). We could detect maximal DNA fragmentation in *Leishmania*
468 cells when exposed to 25 µg/ml of synthesized Ag NPs (Fig. 5B (e)). These promastigotes
469 showed an intense staining (9.78% TUNEL-positive cells) by anti-BrdU as compared with
470 untreated promastigotes (0.34% TUNEL-positive cells) (Fig. 5B (c)).

471 Further detailed analysis of the S phase was done from this same data. By using the dual
472 parameter display method, not only apoptotic cells were resolved but their stage in the cell cycle
473 in term of percentage of DNA content was also determined. R1 gated cells (Fig. 6A) were
474 divided into three sub gates which were R2, R3 and R4 (Fig. 6B). As shown in (Fig. 6C) we
475 further applied markers (M1,M2 and M3) on the sub gates R2, R3 and R4 to denote G2, G3 and
476 G4 ~ depicting pre S phase, S phase and post S phase respectively. As can be seen by the
477 histogram statistics (Fig. 6D) on comparison with the untreated cells, S phase halt was prominent

Antimicrobial Agents and Chemotherapy

478 in cells treated with 25 µg/ml of synthesized Ag NPs (Table 3). Approximately ~3 fold decrease
479 in (percentage of DNA content) S phase of cells treated with synthesized Ag NPs was observed
480 on comparison to untreated cells.

481 The length of S phase was further determined in term of time duration of the S-phase
482 following the protocol of Martynoga et al. (44). Gating was done using forward scatter (FSC)
483 versus side scatter (SSC) in (Fig. 7A). Fluorescence was measured in the log mode using
484 CellQuest Pro software (BD Biosciences, CA), where x-axis depicts BrdU and y-axis depicts PI.
485 Therefore, the ratio between the numbers of cells in the UR quadrants and UL quadrants is equal
486 to the ratio between Ti (which equals 30 min) and Ts when cells are exposed to PI and BrdU. We
487 calculated the time duration of S phase by following the formula:

488 **Ti/Ts= Lcells/Scells ∴Ts = Ti *(Scells/Lcells)**

489 Where L (leaving) cells = $BrdU^-/PI^+$ (these cells in the initial BrdU-labeled S-phase cohort will
490 leave S-phase*)* and Scells = $BrdU^+/PI^+$. Our calculations were based on histograms analysis (Fig.
491 7 B and C) where $BrdU^-/PI^+$ showed in Upper Left quadrant (UL) and $BrdU^+/PI^+$ Upper Right
492 quadrant (UR). Upper Left quadrant (UL) showed ~ 1.47 and 1.16% of PI positive cells in
493 untreated and treated cells respectively and Upper Right quadrant (UR) showed 2.01 and 4.35%
494 of both BrdU and PI positive cells in untreated and treated cells respectively. Our result showed
495 that the time duration of S phase increased in parasites treated with synthesized Ag NPs (1.875
496 h) compared to untreated parasites (0.6836 h). The increased time duration of S phase is
497 responsible for the increased inhibition of proliferation of the cells in this phase. When S phase is
498 lengthened (in term of time duration) the parasites become more disregulated and result in
499 reduced proliferation.

Antimicrobial Agents and Chemotherapy

500 **Formation of ROS in *L. donovani.*** An inherent basic level of ROS production in wild
501 type promastigotes was detected with mean florescence intensity (MFI) of 82.66. Treatment of
502 promastigotes with synthesized Ag NPs for 24 h revealed a gradual decrease of MFI in ROS
503 generation from 34.35, 30.42 and 27.96 at 12.5, 25 and 50 µg/ml, respectively with respect to
504 control cells (Fig. 8A). An established event in most apoptotic cells was the generation of ROS
505 in the cytosol, which directs the cell and its neighboring cells towards the path of apoptotic cell
506 death (45). Lower levels of ROS in our study could be a result of the antioxidant activity of the
507 aqueous leaves extract of *E. prostrata* which constituted the synthesized Ag NPs. Presumably
508 this effect resulted in a shift from apoptosis to G0/G1 arrest followed by necrotic cell death in *L.*
509 *donovani.*

510 **Measurement of intracellular non-protein thiols.** The fluorescent probe, 5-
511 chloromethyl fluorescein diacetate (CMFDA) was used to measure total intracellular non-protein
512 thiols after treatment of *L. donovani* promastigotes with aqueous leaves extract of *E. prostrata*,
513 synthesized Ag NPs and $AgNO_3$ solution. Synthesized Ag NPs showed remarkable decrease in
514 MFI (3.55) in comparison with the control cells (219.69) at 24 h. On analysis of our results we
515 found that intracellular non protein thiols increase in MFI (261.16) in comparison with the wild
516 type cells (219.69) was presumably a result of the antioxidant activity of the aqueous leaves
517 extract of *E. prostrata.* Also, Ag was known to be an excellent effective Trypanothione reductase
518 (TR) inhibitor. In the present observations, $AgNO_3$ treated cells were obtained a remarkable
519 decrease in MFI (5.67) in comparison with the wild type cells (219.69) (Fig. 8B) thus lending
520 credence to the above statement. We infirm that depletion of intracellular non protein thiols in
521 *Leishmania* parasites treated with synthesized Ag NPs was independent of ROS generation. Our
522 study therefore shows the important benefit of taking up these synthesized Ag NPs further for

523 clinical development as our green synthesized NPs has advantage of prevention of development
524 of drug resistance. Since over expression of intracellular non protein thiols in *Leishmania*
525 parasites are a known cause of drug efflux leading to resistance.
526
527 **Discussion**
528
529 Considering the efficacy of drugs available for the treatment of VL as well as their side
530 effects and the resistance developed by parasites, the research in phytosciences, mainly regarding
531 the properties of bioactive phytocompounds found in the crude extracts of medicinal plants, may
532 lead to the discovery of new medicines with appropriate efficiency which are cheap and safe to
533 the patients. The concept of green NPs synthesis was first developed by Raveendran et al. (46).
534 Hence the purpose of this research was to study the antileishmanial effects of synthesized NPs
535 including (Ag) and (TiO_2), on *L. donovani* parasites. The compound, piceatannol isolated from
536 the methanol extracts of another speices of *Euphorbia lagascae* was found moderately active
537 against the promastigotes and more active against amastigotes of *L. donovani* (47). The green
538 leaves of *E. prostrata* were selected for synthesis of NPs because they are the site of
539 photosynthesis and availability of more H^+ ions to reduce the $AgNO_3$ and $TiO(OH)_2$ into Ag and
540 TiO_2 NPs respectively.
541 NPs synthesized either biologically or chemically must be characterized in order to
542 understand their intrinsic properties such as size, monodispersity, aqueous stability, the net
543 charge, adsorption to biomolecules, aggregation and flocculation in various media (48). Our
544 study provided vital information in this regard for both Ag and TiO_2 NPs. The reduction of ions
545 and formation of stable NPs appeared quickly within 6 h of reaction. Characterization via

546 different microscopic techniques (TEM and AFM) and optical spectroscopy (UV-Visible
547 spectroscopy), proved to be a very useful technique for the analysis of NPs. Distinct and fairly
548 broad UV-Vis absorption band of Ag NPs was centered at 420 nm which proved that the NPs
549 were well dispersed without aggregation. The appearance of this band, which was assigned to a
550 surface plasmon, is well documented for various metal NPs with sizes ranging from 2 to 100 nm.
551 Size distribution is a crucial parameter in determining the cellular uptake efficiency of the NPs
552 and their transport through the cellular bilayer. The TEM analysis confirmed the morphological
553 dimension of synthesized Ag NPs using *E. prostrata* were spherical-shape with an average size
554 of 12.82 ± 2.50 nm, *E. prostrata* leaves aqueous extract-mediated synthesized TiO_2 NPs showed
555 circular and irregular shapes and mostly aggregated (thereby probably unable to be transported
556 through the cellular bilayer of the parasite) with an average size of 83.22 ± 1.50 nm.

557 It has been reported that on their own Ag NPs and the plant have antileishmanial property
558 respectively. Our study shows enhanced antileishmanial effect on combination of the two. The
559 antileishmanial activity of synthesized Ag NPs was significantly increased four folds compared
560 to wild type parasites and approximately three folds when just the crude leaves extract or $AgNO_3$
561 solution were used to treat the parasites. The molecular mechanisms for this enhanced
562 antileishmanial synergistic effect of combining $AgNO_3$ solution with aqueous leaves extract of
563 *E. prostrata* were further confirmed by us to be multifactorial (Fig. 9).

564 As has been established by Weingartner et al. (49) that there is no phsophatidylserine, we too
565 confirmed the absence in the proteome of *L. donovani* DD8 (unpublished results). However other
566 phospholipid classes which participate in apoptosis, like phosphatidylethanol sphingomyelin and
567 phosphatidyl choline, can also enable Annexin V staining and therefore Annexin V binding as an
568 early indicator of apoptosis is in use by many other investigators (35, 50). Our results of annexin

569 V- FITC and PI indicated necrosis as shift from upper right (UR) to upper left (UL) quadrant of
570 synthesized Ag NPs treated parasites. Ultrastructural analysis was also indicative of necrosis.
571 Initially DNA fragmentation as detected by TUNEL indicated apoptosis. However high
572 molecular weight DNA fragmentation observed by gel electrophoresis are indicative for necrotic
573 cell death (51).

574 Arrest of cell cycle in G0/G1 phase led to S phase halt and the inhibition of the
575 proliferation of the parasites. We monitored S phase progression in promastigotes treated with or
576 without synthesized Ag NPs by flow cytometry following the method of Wheeler et al. (52)
577 where it has been described that S phase can be monitored by either cell cycle progression,
578 microscope cytometry, flow cytometry, K/N configuration counts and short-pulse BrdU. In
579 synthesized Ag NPs treated parasites, the length of S phase (pre S, S and post S phase) appeared
580 particularly short in term of percentage DNA content in comparison with untreated cells, leading
581 to the inhibition of proliferation.

582 We found decreased ROS production in the synthesized Ag NPs treated parasites which
583 is responsible for caspase independent necrotic cell death mechanism. Although nanoparticles
584 have antimicrobial activity, however, silver and titanium dioxide nanoparticles are also known to
585 induce oxidative stress *in vitro* and *in vivo* (53). In our study the plant extract of *E. prostrata* and
586 synthesized Ag NPs were found to possess maximum antioxidant activity. The main chemical
587 constituent of plant extract of *E. prostrata* is 2,3-dihydrobenzofuran which is a known
588 antioxidant (54). High level of intracellular non protein thiol in *E. prostrata* plant extract treated
589 parasites as compared to almost negligible level in $AgNO_3$ and synthesized Ag NPs treated
590 parasites could be responsible for the quenching of ROS. Because the low thiol levels within the
591 cells treated with synthesized Ag NPs do not lead to adduct formation of efflux.

592 In *L. donovani* the glutathione/glutathione reductase eukaryotic redox system replaced by
593 the unique trypanothione/trypanothione reductase (TR) system. Ag NPs is known to be an
594 excellent effective TR inhibitor (55). This was also corroborated by our results which showed
595 maximum TR inhibition in synthesized Ag NPs treated promastigotes in comparison to aqueous
596 leaves extract of *E. prostrata* treated promastigotes. This can have an important implication in
597 the treatment of clinical drug resistance with synthesized Ag NPs. It has been established that
598 2,3-dihydrobenzofuran, the main chemical constituent of plant extract of *E. prostrata*, is also a
599 promising antileishmanial lead molecule and contains antitubulin properties (56). This drug
600 target of the parasite has a different primary amino acid sequence to that of its host. In
601 conclusion we can affirm from our studies that the synthesized Ag NPs could have a dual mode
602 of leishmanicidal activity by targeting tubulins (dihydrobenzofuran of aqueous leaves extract of
603 *E. prostrata*) or trypanothione/trypanothione reductase (TR) (Ag NPs).

604

605 **Acknowledgments**

606 The authors are grateful to C. Abdul Hakeem College Management, Dr. K. Masood Ahmed
607 Principal, and Dr. Hameed Abdul Razack, Head of Zoology Department for providing the
608 facilities to carry out this work. The technical assistance of Mr. A.L. Vishwakarma regarding
609 flow cytometry is acknowledged. This work was supported by Council of Scientific and
610 Industrial Research (CSIR) funded network project "Host Interactome analysis: Understanding
611 the Role of Host molecules in Parasitic Infection (HOPE)." This is CDRI communication no.
612 8767.

613

614 **Conflict of Interest**

615 The authors declare no conflict of interest.

616

617 **References**

618

619 1. **Desjeux P.** 2004. Leishmaniasis: current situation and new perspectives. Comparative
620 immunology, microbiology and infectious diseases **27:**305-318.
621 2. **Richard JV, Werbovetz KA.** 2010. New antileishmanial candidates and lead
622 compounds. Current opinion in chemical biology **14:**447-455.
623 3. **Ezra N, Ochoa MT, Craft N.** 2010. Human immunodeficiency virus and leishmaniasis.
624 Journal of global infectious diseases **2:**248.
625 4. **Kim BY, Rutka JT, Chan WC.** 2010. Nanomedicine. New England Journal of
626 Medicine **363:**2434-2443.
627 5. **Irache JM, Esparza I, Gamazo C, Agüeros M, Espuelas S.** 2011. Nanomedicine:
628 novel approaches in human and veterinary therapeutics. Veterinary parasitology **180:**47-
629 71.
630 6. **Morones JR, Elechiguerra JL, Camacho A, Holt K, Kouri JB, Ramírez JT,**
631 **Yacaman MJ.** 2005. The bactericidal effect of silver nanoparticles. Nanotechnology
632 **16:**2346.
633 7. **Sinha S, Pan I, Chanda P, Sen SK.** 2009. Nanoparticles fabrication using ambient
634 biological resources. J Appl Biosci **19:**1113-1130.
635 8. **Bhainsa KC, D'souza S.** 2006. Extracellular biosynthesis of silver nanoparticles using
636 the fungus< i> *Aspergillus fumigatus*</i>. Colloids and Surfaces B: Biointerfaces
637 **47:**160-164.

638 9. **Mohebali M, Rezayat M, Gilani K, Sarkar S, Akhoundi B, Esmaeili J, Satvat T,**
639 **Elikaee S, Charehdar S, Hooshyar H.** 2009. Nanosilver in the treatment of localized
640 cutaneous leishmaniasis caused by *Leishmania major* (MRHO/IR/75/ER): an *in vitro* and
641 *in vivo* study. DARU Journal of Pharmaceutical Sciences **17:**285-289.

642 10. **Zampa MF, Araujo I, Costa V, Nery Costa CH, Santos Jr JR, Zucolotto V, Eiras C,**
643 **Leite JRS.** 2009. Leishmanicidal Activity and Immobilization of dermaseptin 01
644 antimicrobial peptides in ultrathin films for nanomedicine applications. Nanomedicine:
645 Nanotechnology, Biology and Medicine **5:**352-358.

646 11. **Allahverdiyev AM, Abamor ES, Bagirova M, Ustundag CB, Kaya C, Kaya F,**
647 **Rafailovich M.** 2011. Antileishmanial effect of silver nanoparticles and their enhanced
648 antiparasitic activity under ultraviolet light. International journal of nanomedicine
649 **6:**2705.

650 12. **Torabi N, Mohebali M, Shahverdi AR, Rezayat SM, Edrissian GH, Esmaeili J,**
651 **Charehdar S.** 2011. Nanogold for the treatment of zoonotic cutaneous leishmaniasis
652 caused by *Leishmania major* (MRHO/IR/75/ER): An animal trial with methanol extract
653 of *Eucalyptus camaldulensis*. JOURNAL OF PHARMACEUTICAL.

654 13. **Navarro L, Dunoyer P, Jay F, Arnold B, Dharmasiri N, Estelle M, Voinnet O, Jones**
655 **JD.** 2006. A plant miRNA contributes to antibacterial resistance by repressing auxin
656 signaling. Science **312:**436-439.

657 14. **Wiesenthal A, Hunter L, Wang S, Wickliffe J, Wilkerson M.** 2011. Nanoparticles:
658 small and mighty. International journal of dermatology **50:**247-254.

659 15. **Das S, Roy P, Mondal S, Bera T, Mukherjee A.** 2013. One pot synthesis of gold
660 nanoparticles and application in chemotherapy of wild and resistant type visceral
661 leishmaniasis. Colloids and Surfaces B: Biointerfaces **107:**27-34.
662 16. **Sundrarajan M, Gowri S.** 2011. Green synthesis of titanium dioxide nanoparticles by
663 *Nyctanthes arbor-tristis* leaves extract. Chalcogenide Letters **8:**447-451.
664 17. **Schmelzer GH, Gurib-Fakim A.** 2008. Medicinal plants 1. PROTA Foundation.
665 18. **Rene K, Hortense GK, Pascal W, Jean Alexis M, Vidal PE, Michel Archange F,**
666 **Christine FM.** 2007. Activity of aqueous ethanol extract of *Euphorbia prostrata* ait on
667 *Shigella dysenteriae* type 1-induced diarrhea in rats. Indian Journal of Pharmacology
668 **39:**240.
669 19. **Kerboeuf D, Riou M, Guégnard F.** 2008. Flavonoids and related compounds in
670 parasitic disease control. Mini reviews in medicinal chemistry **8:**116-128.
671 20. **Radtke OA, Foo LY, Lu Y, Kiderlen AF, Kolodziej H.** 2003. Evaluation of sage
672 phenolics for their antileishmanial activity and modulatory effects on interleukin-6,
673 interferon and tumour necrosis factor-alpha-release in RAW 264.7 cells. Zeitschrift fur
674 Naturforschung C **58:**395-400.
675 21. **Sharma U, Singh D, Kumar P, Dobhal M, Singh S.** 2011. Antiparasitic activity of
676 plumericin & isoplumericin isolated from *Plumeria bicolor* against *Leishmania donovani*.
677 The Indian journal of medical research **134:**709.
678 22. **Parashar V, Parashar R, Sharma B, Pandey AC.** 2009. *Parthenium* leaf extract
679 mediated synthesis of silver nanoparticles: a novel approach towards weed utilization.
680 Digest journal of nanomaterials and biostructures **4:**45-50.

681 23. **Veerasamy R, Xin TZ, Gunasagaran S, Xiang TFW, Yang EFC, Jeyakumar N,**
682 **Dhanaraj SA.** 2011. Biosynthesis of silver nanoparticles using mangosteen leaf extract
683 and evaluation of their antimicrobial activities. Journal of Saudi Chemical Society
684 **15:**113-120.
685 24. **Horcas I, Fernandez R, Gomez-Rodriguez J, Colchero J, Gómez-Herrero J, Baro A.**
686 2007. WSXM: a software for scanning probe microscopy and a tool for nanotechnology.
687 Review of Scientific Instruments **78:**013705.
688 25. **Ausloos P, Clifton C, Lias S, Mikaya A, Stein S, Tchekhovskoi D, Sparkman O,**
689 **Zaikin V, Zhu D.** 1999. The critical evaluation of a comprehensive mass spectral library.
690 Journal of the American Society for Mass Spectrometry **10:**287-299.
691 26. **Kaur J, Kumar P, Tyagi S, Pathak R, Batra S, Singh P, Singh N.** 2011. In silico
692 screening, structure-activity relationship, and biologic evaluation of selective pteridine
693 reductase inhibitors targeting visceral leishmaniasis. Antimicrobial agents and
694 chemotherapy **55:**659-666.
695 27. **Kaur J, Sundar S, Singh N.** 2010. Molecular docking, structure–activity relationship
696 and biological evaluation of the anticancer drug monastrol as a pteridine reductase
697 inhibitor in a clinical isolate of *Leishmania donovani*. Journal of antimicrobial
698 chemotherapy **65:**1742-1748.
699 28. **Ghosh S, Debnath S, Hazra S, Hartung A, Thomale K, Schultheis M, Kapkova P,**
700 **Schurigt U, Moll H, Holzgrabe U.** 2011. *Valeriana wallichii* root extracts and fractions
701 with activity against *Leishmania* spp. Parasitology research **108:**861-871.

29. **Wong IL, Chan K-F, Chen Y-F, Lun Z-R, Chan TH, Chow LM.** 2014. *In vitro* and *in vivo* efficacy of novel flavonoid dimers against cutaneous leishmaniasis. Antimicrobial agents and chemotherapy**:**AAC. 02425-02413.

30. **Chouhan G, Islamuddin M, Ahmad F, Sahal D, Afrin F.** 2014. Antileishmanial Potential of *Piper nigrum* Seed Extracts against *Leishmania donovani*. Open Journal of Medical Microbiology **4:**228.

31. **Maria do Socorro SR, Mendonça-Filho RR, Bizzo HR, de Almeida Rodrigues I, Soares RMA, Souto-Padrón T, Alviano CS, Lopes AHC.** 2003. Antileishmanial activity of a linalool-rich essential oil from *Croton cajucara*. Antimicrobial agents and chemotherapy **47:**1895-1901.

32. **Gould MK, Vu XL, Seebeck T, de Koning HP.** 2008. Propidium iodide-based methods for monitoring drug action in the kinetoplastidae: comparison with the Alamar Blue assay. Analytical biochemistry **382:**87-93.

33. **Gaur U, Showalter M, Hickerson S, Dalvi R, Turco SJ, Wilson ME, Beverley SM.** 2009. < i> *Leishmania donovani*</i> lacking the Golgi GDP-Man transporter< i> LPG2</i> exhibit attenuated virulence in mammalian hosts. Experimental parasitology **122:**182-191.

34. **Kaur J, Singh BK, Tripathi RP, Singh P, Singh N.** 2009. < i> *Leishmania donovani*</i>: A glycosyl dihydropyridine analogue induces apoptosis like cell death via targeting pteridine reductase 1 in promastigotes. Experimental parasitology **123:**258-264.

35. **Marinho FA, Gonçalves KC, Oliveira SS, Gonçalves DS, Matteoli FP, Seabra SH, Oliveira ACS, Bellio M, Oliveira SS, Souto-Padrón T.** 2014. The Calpain Inhibitor

Antimicrobial Agents and Chemotherapy

MDL28170 Induces the Expression of Apoptotic Markers in *Leishmania amazonensis* Promastigotes. PloS one **9:**e87659.

36. **Mukherjee SB, Das M, Sudhandiran G, Shaha C.** 2002. Increase in cytosolic Ca2+ levels through the activation of non-selective cation channels induced by oxidative stress causes mitochondrial depolarization leading to apoptosis-like death in *Leishmania donovani* promastigotes. Journal of Biological Chemistry **277:**24717-24727.

37. **Sarkar A, Mandal G, Singh N, Sundar S, Chatterjee M.** 2009. Flow cytometric determination of intracellular non-protein thiols in< i> *Leishmania*</i> promastigotes using 5-chloromethyl fluorescein diacetate. Experimental parasitology **122:**299-305.

38. **Dubey M, Bhadauria S, Kushwah B.** 2009. Green synthesis of nanosilver particles from extract of *Eucalyptus hybrida* (safeda) leaf. Dig J Nanomater Bios **4:**537-543.

39. **Liu Z, Hong L, Guo B.** 2005. Physicochemical and electrochemical characterization of anatase titanium dioxide nanoparticles. Journal of power sources **143:**231-235.

40. **Coates J.** 2000. Interpretation of infrared spectra, a practical approach. Encyclopedia of analytical chemistry.

41. **Logeswari P, Silambarasan S, Abraham J.** 2012. Synthesis of silver nanoparticles using plants extract and analysis of their antimicrobial property. Journal of Saudi Chemical Society.

42. **Kaur J, Dutta S, Chang K-P, Singh N.** 2013. A member of the Ras oncogene family, RAP1A, mediates antileishmanial activity of monastrol. Journal of Antimicrobial Chemotherapy **68:**1071-1080.

43. **Efuet ET, Keyomarsi K.** 2006. Farnesyl and geranylgeranyl transferase inhibitors induce G1 arrest by targeting the proteasome. Cancer research **66:**1040-1051.

Antimicrobial Agents and Chemotherapy

747 44. **Martynoga B, Morrison H, Price DJ, Mason JO.** 2005. Foxg1 is required for
748 specification of ventral telencephalon and region-specific regulation of dorsal
749 telencephalic precursor proliferation and apoptosis. Developmental biology **283:**113-127.
750 45. **Chipuk JE, Green DR.** 2005. Do inducers of apoptosis trigger caspase-independent cell
751 death? Nature Reviews Molecular Cell Biology **6:**268-275.
752 46. **Raveendran P, Fu J, Wallen SL.** 2006. A simple and "green" method for the synthesis
753 of Au, Ag, and Au–Ag alloy nanoparticles. Green Chem **8:**34-38.
754 47. **Duarte N, Kayser O, Abreu P, Ferreira MJU.** 2008. Antileishmanial activity of
755 piceatannol isolated from *Euphorbia lagascae* seeds. Phytotherapy Research **22:**455-457.
756 48. **McNeil SE.** 2011. Characterization of nanoparticles intended for drug delivery. Springer.
757 49. **Weingärtner A, Kemmer G, Müller FD, Zampieri RA, dos Santos MG, Schiller J,**
758 **Pomorski TG.** 2012. *Leishmania* promastigotes lack phosphatidylserine but bind
759 annexin V upon permeabilization or miltefosine treatment. PloS one **7:**e42070.
760 50. **Chowdhury S, Mukherjee T, Chowdhury SR, Sengupta S, Mukhopadhyay S,**
761 **Jaisankar P, Majumder HK.** 2014. Disuccinyl Betulin Triggers Metacaspase-
762 Dependent Endonuclease G-Mediated Cell Death in Unicellular Protozoan Parasite
763 Leishmania donovani. Antimicrobial agents and chemotherapy **58:**2186-2201.
764 51. **Bicknell GR, Cohen GM.** 1995. Cleavage of DNA to large kilobase pair fragments
765 occurs in some forms of necrosis as well as apoptosis. Biochemical and biophysical
766 research communications **207:**40-47.
767 52. **Wheeler RJ, Gluenz E, Gull K.** 2011. The cell cycle of *Leishmania:* morphogenetic
768 events and their implications for parasite biology. Molecular microbiology **79:**647-662.

53. **Ganapathi AP, Devaki R, Thuniki NR, Manna J, Tirumuru B, Gopu CR, Deepthi SB, Trivedi R, Rana RK, Hasan A.** 2014. *In vitro* assessment of Ag and TiO2 nanoparticles cytotoxicity. International Journal of Research in Medical Sciences **2:**1360-1367.

54. **Chen C-H, Chen C-H, Shaw C-Y, Chen C-C, Tsai Y-C.** 2002. 2, 3, 4-Trimethyl-5, 7-dihydroxy-2, 3-dihydrobenzofuran, a novel antioxidant, from *Penicillium citrinum* F5. Journal of natural products **65:**740-741.

55. **Baiocco P, Ilari A, Ceci P, Orsini S, Gramiccia M, Di Muccio T, Colotti G.** 2010. Inhibitory effect of silver nanoparticles on trypanothione reductase activity and *Leishmania infantum* proliferation. ACS Medicinal Chemistry Letters **2:**230-233.

56. **Miert SV, Dyck SV, Schmidt TJ, Brun R, Vlietinck A, Lemière G, Pieters L.** 2005. Antileishmanial activity, cytotoxicity and QSAR analysis of synthetic dihydrobenzofuran lignans and related benzofurans. Bioorganic & medicinal chemistry **13:**661-669.

Antimicrobial Agents and Chemotherapy

792 **Table 1:** Chemical composition of the *E. prostrata* leaves extract identified by GC-MS.

RT	Identified molecules	Chemical structure	MF	MW	Peak area %
3.3	2,3-dihydrobenzofuran	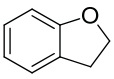	C_8H_8O	120	27.44
4.3	1,3- dihydro isobenzofuran	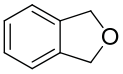	C_8H_8O	120	19.97
18.5	4- cholro-2,5-dimethoxybenzamine	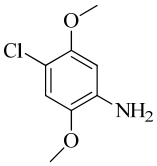	$C_9H_{10}ClNO_2$	187	21.80
22.6	Methyl 3-(hydromethyl)bicycle [3.2.1]oct-6-ene-1-carboxylate	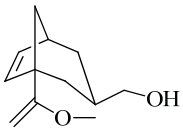	$C_{10}H_{14}O_3$	182	5.53

793

794 RT: Retention time; MF: Molecular formula; MW: Molecular weight.

795

796

797

798

799

800

801 **Table 2:** The mean % cell viability test by one way ANOVA and Dunnett`s multiple comparison
802 test.

Factor	**Mean**	**Standard deviation**	**p-value**
Ag NPs	0.255	0.015	$p<0.001$
TiO_2 NPs	0.653	0.001	$p<0.001$
Aqueous extract	0.359	0.007	$p<0.001$
$AgNO_3$	0.320	0.003	$p<0.01$
$TiO(OH)_2$	0.747	0.018	$p<0.001$
Control	0.989	0.016	$p<0.001$

803

804 The significance between synthesized Ag NPs and aqueous leaves extract of *E. prostrata*,
805 $AgNO_3$, and $TiO(OH)_2$ solutions and synthesized TiO_2 NPs (Factor). Lowest percentage cell
806 viability was found with synthesized Ag NPs. It was significantly lower than all other factor.

807

808

809

810

811

812

813

814

815

816 **Figure Legends**

817

818 **Figure 1. [A]** Characterization of synthesized (Ag and TiO_2) NPs (a) XRD pattern of Ag NPs
819 synthesized by using *E. Prostrata.* (b) Shows XRD pattern of TiO_2 NPs synthesized by using *E.*
820 *prostrata.* **[B]** (a) FTIR spectra of vacuum dried powder of synthesized Ag NPs from *E.*
821 *Prostrata.* (b) FTIR spectra of vacuum dried powder of synthesized TiO_2 NPs from aqueous leaf
822 extracts of *E. prostrata*.

823 **Figure 2. [A]** Shows the atomic micrograph of synthesized Ag NPs with (a) aerial and (b) 3D
824 topographical view of the topological structures. **[B]** Shows the atomic micrograph of
825 synthesized TiO_2 NPs with (a) aerial and (b) 3D topographical view of the topological structures.
826 **[C]** Transmission electron microscopy (TEM) micrograph showing size, shape and morphology
827 of synthesized NPs. TEM images of the synthesized Ag NPs (a, b) and (c) SAED (selected area
828 electron diffraction). **[D]** TEM images of the synthesized TiO_2 NPs (a, b) and (c) SAED.

829 **Figure 3. [A]** Cell viability assessment by alamarBlue® shows reduction in viability with
830 different concentrations (0, 12.5, 25, 50 and 100 µg/ml) of synthesized Ag NPs treated
831 promastigotes. (a) Graph shows that the synthesized Ag NPs were most active against
832 promastigotes of *L. donovani* compared to aqueous extract of *E. prostrata* leaves, $AgNO_3$
833 solution, $TiO(OH)_2$, synthesized TiO_2 NPs and control. (b) Microscopic images of wild type
834 promastigotes and promastigotes treated with aqueous leaves extract of *E. prostrata*, AgNO3
835 solution and synthesized Ag NPs. Magnification x 60. (c) Percentage cell viability against log
836 value of synthesized Ag NPs concentrations (µg/ml), IC_{50} = 14.94 µg/ml. (d) Percentage cell
837 viability of *L. donovani* promastigotes treated with synthesized Ag NPs concentrations. The data
838 are presented as mean ± standard deviation of three independent experiments. **[B]** *In vitro*

839 analysis of antileishmanial activity of synthesized Ag NPs (a) **in intracellular amastigotes**
840 **(IC_{50}):** Macrophages (4000 cells/well, final volume 200 µl) were infected with promastigotes of
841 *L. donovani* in a ratio of 6:1 (parasites/macrophages) and infected macrophages were treated
842 with increasing concentrations (0, 2.5, 5 and 10 µg/ml) of synthesized Ag NPs for 24 h. After
843 indicated incubation time, treated or untreated cells were stained with Giemsa stain and the slides
844 were viewed on an inverted bright field microscope (IX73 Inverted Microscope, Olympus). The
845 50% inhibitory concentration (IC_{50}) was obtained by plotting the graph of percentage of cell
846 viability versus different concentrations of synthesized Ag NPs. The results were taken as the
847 mean of duplicate experiments. (b) **cytotoxicity in macrophages (CC_{50}):** Macrophages (50,000
848 cells/well, final volume 200 µl) were treated with increasing concentrations (0, 5, 10 and 20
849 µg/ml) of synthesized Ag NPs for 24 h. After indicated incubation time, the viability of the
850 macrophages was estimated by MTT [3-(4,5-dimethylthiazole-2-yl)-2-5-diphenyl tetrazolium
851 bromide] assay. The 50% cytotoxic concentration (CC_{50}) was determined by logarithmic
852 regression analysis using GraphPrism 5 software. Results are presented as mean ± SD; n=3. **[C]**
853 Transmission electron microscopy of *L. donovani* promastigotes incubated with vehicle (a, b and
854 c) and synthesized Ag NPs (d, e and f) at IC_{50} dose for 45 min, n: nucleus; k: kinetoplast; m:
855 mitrochondria; pf: pocket flagellar; pm: plasma membrane; G: golgi body; g: glycosome; ER:
856 endoplasmic reticulum. Scale bars 1.0 µm and 0.5 µm.

857 **Figure 4. [A]** PI uptake analysis: Dot plots (a, b, c and d) show that treatment of *Leishmania*
858 parasites with synthesized Ag NPs leads to (PI-positive cells M2) (a1, b1, c1 and d1) cell death
859 in a concentration-dependent manner (e). **[B]** Externalization of phosphatidylserine in
860 synthesized Ag NPs treated promastigotes. *L. donovani* promastigotes were incubated with
861 different concentrations of synthesized Ag NPs (0, 12.5, 25 and 50 µg/ml, (a-d)) for 24 h and

862 analysed by flow cytometry. After indicated incubation time, a significant number of membrane
863 compromised cells were stained positively by annexin V- FITC, PI (upper-right quadrant) and
864 only PI positive (upper-left quardrant). (e) Graph showing percentage population of live,
865 apoptotic and necrotic state of treated parasites. **[C]** Synthesized Ag NPs induced cell cycle
866 arrest in the G0/G1 phase of *L. donovani* parasites. After treatment with different concentrations
867 of synthesized Ag NPs (0, 12.5, 25 and 50 µg/ml, (a-d)) for 24 h, promastigotes were collected,
868 washed with PBS and stained with PI, the DNA content was analysed by flow cytometry. (e)
869 Graph showing % population in G0/G1, S and G2/M phase of treated parasites. (f) DNA
870 fragmentation of *L. donovani* promastigotes treated with different concentrations of synthesized
871 Ag NPs (12.5, 25 and 50 µg/ml). M represents DNA ladder, Lane 1 shows DNA from untreated
872 cells while Lane 2, 3 and 4 represent DNA from synthesized Ag NPs treated cells. The data are
873 presented as mean ± standard deviation of three independent experiments.

874 **Figure 5.** Synthesized Ag NPs-induced DNA fragmentation in promastigotes of *L. donovani* was
875 analysed by TUNEL assay using flow cytometry. **[A]** Gating was done within the DNA Area on
876 the y-axis (FL2-A) and the DNA Width on the x-axis (FL2-W). **[B]** A gate was drawn around the
877 non -clumped cells. Where the x-axis depicts DNA (FL2 channel) and the y-axis depicts Anti-
878 BrdU-FITC (FL1 channel). Increasing concentrations of synthesized Ag NPs showed the
879 increase number of cells (R2) stained by anti-BrdU which have moved from non apoptotic
880 population (G0/G1 and G2 phase) to the apoptotic population (S phase). (a) and (b) represent
881 negative and positive control respectively (provided by kit) where (c), (d), (e) and (f) show
882 promastigotes treated with different concentrations (0, 12.5, 25 and 50 µg/ml) of synthesized Ag
883 NPs respectively.

884 **Figure 6.** The length of S phase varies according to the percentage of DNA content in untreated
885 and treated promastigotes of *L. donovani.* By using the dual parameter display method **[A]** A
886 gate was drawn around the non -clumped cells (R1) and **[B]** R1 gated cells were divided into
887 three sub gates which were R2, R3 and R4. **[C]** We further applied markers (M1,M2 and M3) on
888 the sub gates R2, R3 and R4 to denote G2, G3 and G4 ~ depicting pre S phase, S phase and post
889 S phase respectively. **[D]** Show the statistics analysis of sub gated cells of *L. donovani*. **(Table 3)**
890 S phase halt (in term of percentage of DNA content) was prominent in cells treated with 25
891 µg/ml of synthesized Ag NPs as compared to untreated cells. Where (c) and (e) denote untreated
892 parasites and parasites treated with 25 µg/ml of synthesized Ag NPs respectively.

893 **Figure 7.** The length of S phase in term of time duration was determined by double labeling
894 method: **[A]** Gating was done using forward scatter (FSC) versus side scatter (SSC). **[B and C]**
895 Fluorescence was measured in the log mode using CellQuest Pro software (BD Biosciences,
896 CA). Where x-axis depicts BrdU and y-axis depicts PI. **[B]** Represents the histogram of untreated
897 promastigotes and **[C]** represents the histogram of treated (with 25 µg/ml of synthesized Ag
898 NPs) promastigotes respectively.

899 **Figure 8. [A]** ROS generation was measured using the fluorescent dye 2,7
900 dichlorodihydrofluorescein diacetate after treatment with (a) different concentrations (12.5, 25
901 and 50 µg/ml) of synthesized Ag NPs for 24 h and its fluorescence was measured using a flow
902 cytometer. (b) Graph shows mean fluorescence intensity of DCF in control and synthesized Ag
903 NPs treated cells at 24 h. The data are presented as mean ± standard deviation of three
904 independent experiments. **[B]** Intracellular level of the glutathione (GSH) in *L. donovani*
905 promastigotes treated with *E.prostrata*, $AgNO_3$solution and synthesized Ag NPs. (b) Graph
906 shows mean fluorescence intensity of CMF (GSH sensitive probe) in control, *E. prostrata,*

Antimicrobial Agents and Chemotherapy

907 $AgNO_3$ and synthesized Ag NPs treated cells at 24 h. The data are presented as mean ± standard
908 deviation of three independent experiments.

909 **Figure 9.** Schematic diagram of proposed mechanism of synthesized Ag NPs induced cell death
910 in *L. donovani* promastigotes. Synthesized Ag NPs inhibit promastigotes proliferation and
911 induced caspase independent cell death which is largely due to necrosis. Cell death in *L.*
912 *donovani* promastigotes is accompanied by decreased level of intracellular non-protein thiols and
913 reactive oxygen species.

914

915

916

917

918

919

920

921

922

923

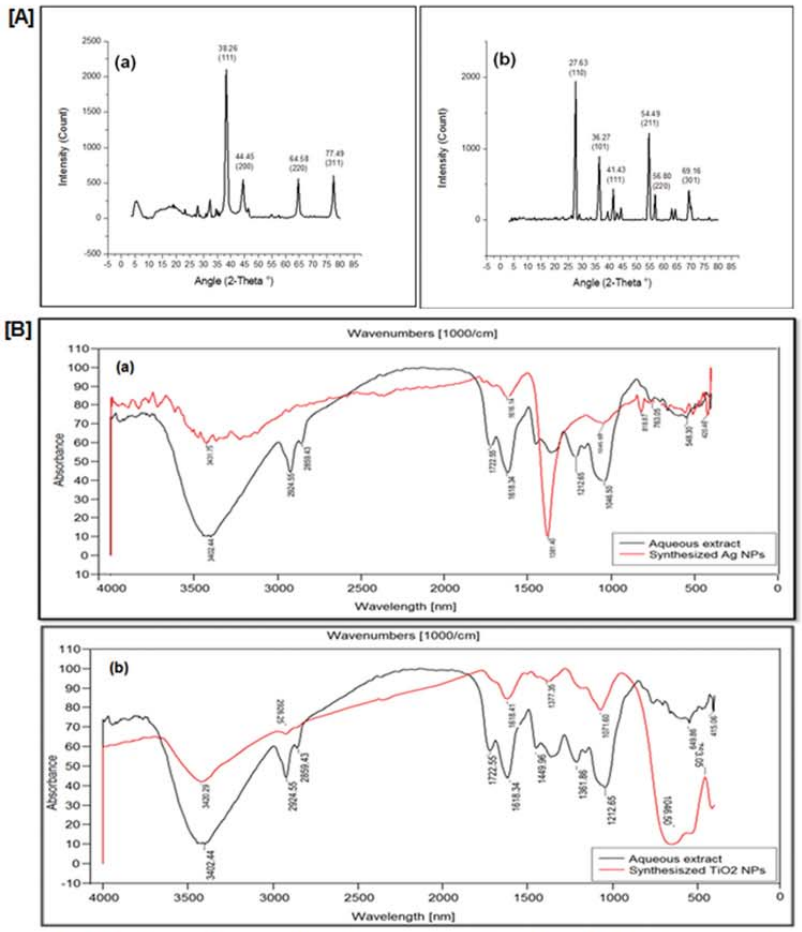

Figure 1. [A] Characterization of synthesized (Ag and TiO_2) NPs (a) XRD pattern of Ag NPs synthesized by using *E. Prostrata*. (b) Shows XRD pattern of TiO_2 NPs synthesized by using *E. prostrata*. **[B]** (a) FTIR spectra of vacuum dried powder of synthesized Ag NPs from *E. Prostrata*. (b) FTIR spectra of vacuum dried powder of synthesized TiO_2 NPs from aqueous leaf extracts of *E. prostrata*.

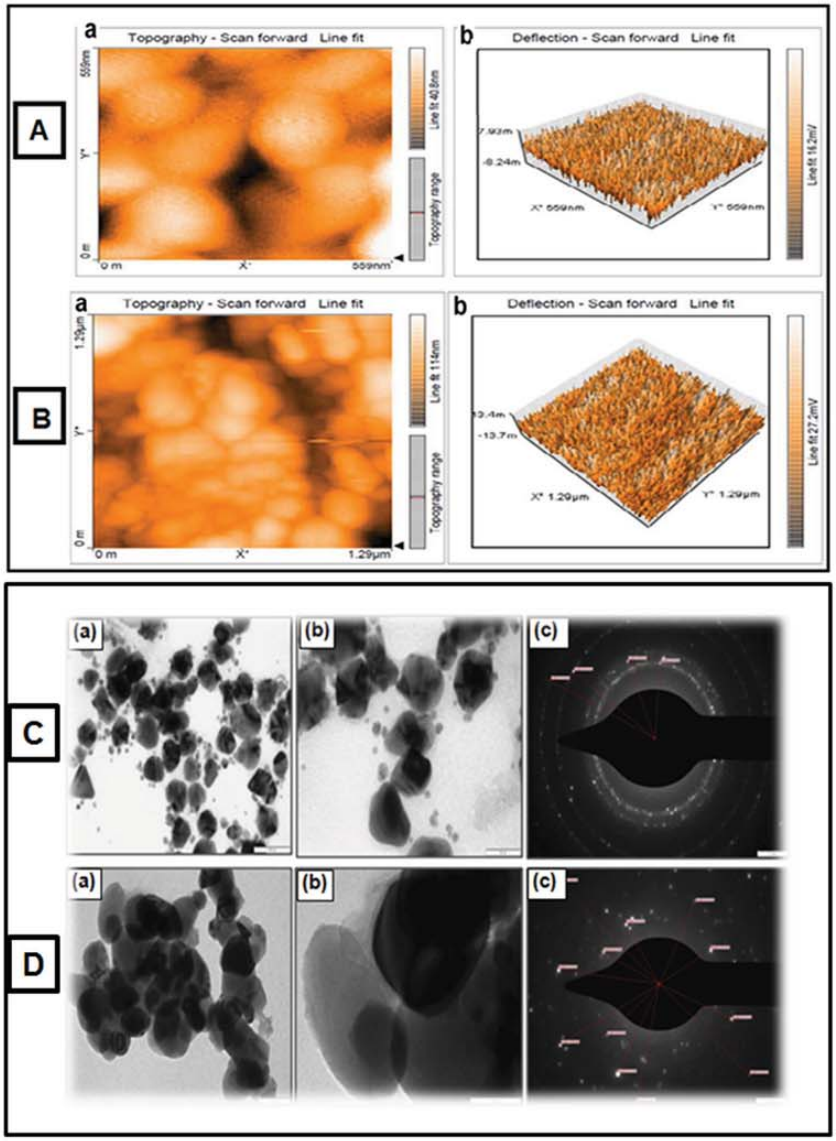

Figure 2. (A) Shows the atomic micrograph of synthesized Ag NPs with [a] aerial and [b] 3D topographical view of the topological structures. **(B)** Shows the atomic micrograph of synthesized TiO_2 NPs with [a] aerial and [b] 3D topographical view of the topological structures. **(C)** Transmission electron microscopy (TEM) showing size, shape and morphology of synthesized NPs. TEM images of the synthesized Ag NPs [a, b] and [c] SAED (selected area electron diffraction). **(D)** TEM images of the synthesized TiO_2 NPs [a, b] and [c] SAED.

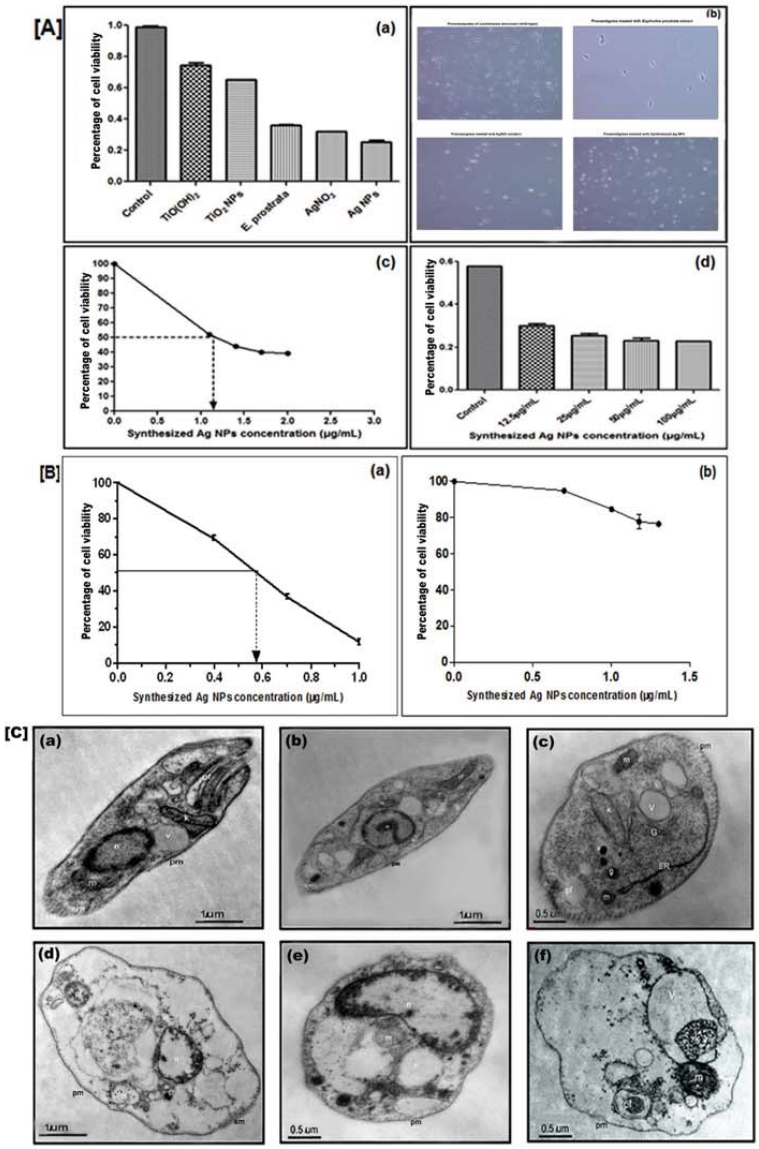

Figure 3. [A] Cell viability assessment by alamarBlue® shows reduction in viability with different concentrations (0, 12.5, 25, 50 and 100 µg/ml) of synthesized Ag NPs treated promastigotes. (a) Graph shows that the synthesized Ag NPs were most active against promastigotes of *L. donovani* compared to aqueous extract of *E. prostrata* leaves, $AgNO_3$ solution, $TiO(OH)_2$, synthesized TiO_2 NPs and control. (b) Microscopic images of wild type promastigotes and promastigotes treated with aqueous leaves extract of *E. prostrata*, AgNO3 solution and synthesized Ag NPs. Magnification x 60. (c) Percentage cell viability against log value of synthesized Ag NPs concentrations (µg/ml), IC_{50} = 14.94 µg/ml. (d) Percentage cell viability of *L. donovani* promastigotes treated with synthesized Ag NPs concentrations. The data are presented as mean ± standard deviation of three independent experiments. **[B]** *In vitro* analysis of antileishmanial activity of synthesized Ag NPs (a) **in intracellular amastigotes (IC_{50}):** Macrophages (4000 cells/well, final volume 200 µl) were infected with promastigotes of *L. donovani* in a ratio of 6:1 (parasites/macrophages) and infected macrophages were treated with increasing concentrations (0, 2.5, 5 and 10 µg/ml) of synthesized Ag NPs for 24 h. After indicated incubation time, treated or untreated cells were stained with Giemsa stain and the slides were viewed on an inverted bright field microscope (IX73 Inverted Microscope, Olympus). The 50% inhibitory concentration (IC_{50}) was obtained by plotting the graph of percentage of cell viability versus different concentrations of synthesized Ag NPs. The results were taken as the mean of duplicate experiments. (b) **cytotoxicity in macrophages (CC_{50}):** Macrophages (50,000 cells/well, final volume 200 µl) were treated with increasing concentrations (0, 5, 10 and 20 µg/ml) of synthesized Ag NPs for 24 h. After indicated incubation time, the viability of the macrophages was estimated by MTT [3-(4,5-dimethylthiazole-2-yl)-2-5-diphenyl tetrazolium bromide] assay. The 50% cytotoxic concentration (CC_{50}) was determined by logarithmic regression analysis using GraphPrism 5 software. Results are presented as mean ± SD; n=3. **[C]** Transmission electron microscopy of *L. donovani* promastigotes incubated with vehicle (a, b and c) and synthesized Ag NPs (d, e and f) at IC_{50} dose for 45 min, n: nucleus; k: kinetoplast; m: mitrochondria; pf: pocket flagellar; pm: plasma membrane; G: golgi body; g: glycosome; ER: endoplasmic reticulum. Scale bars 1.0 µm and 0.5 µm.

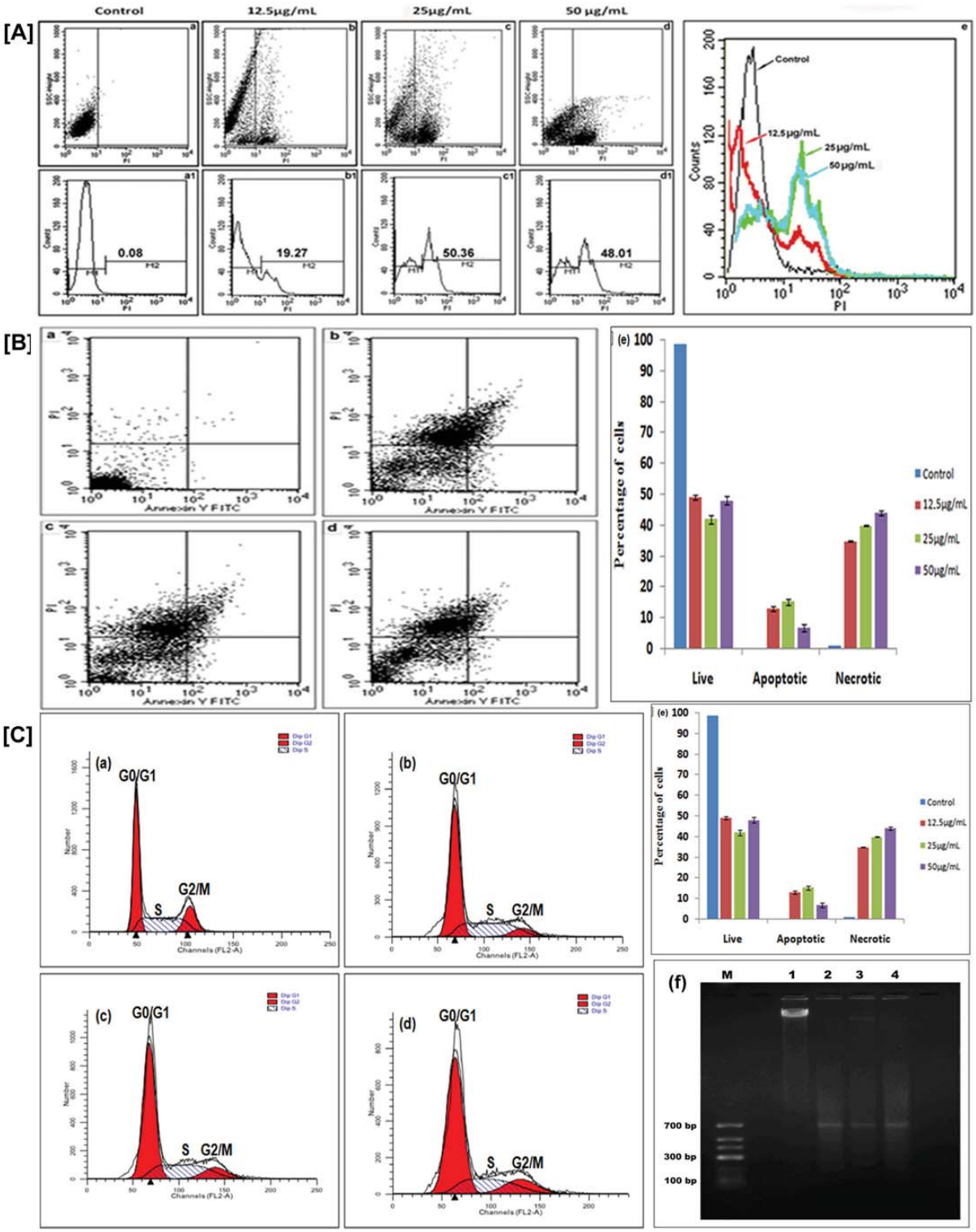

Figure 4. [A] PI uptake analysis: Dot plots (a, b, c and d) show that treatment of *Leishmania* parasites with synthesized Ag NPs leads to (PI-positive cells M2) (a1, b1, c1 and d1) cell death in a concentration-dependent manner (e). **[B]** Externalization of phosphatidylserine in synthesized Ag NPs treated promastigotes. *L. donovani* promastigotes were incubated with different concentrations of synthesized Ag NPs (0, 12.5, 25 and 50 µg/mL, (a-d)) for 24 h and analysed by flow cytometry. After indicated incubation time, a significant number of membrane compromised cells were stained positively by annexin V- FITC, PI (upper-right quadrant) and only PI positive (upper-left quardrant). (e) Graph showing percentage population of live, apoptotic and necrotic state of treated parasites. **[C]** Synthesized Ag NPs induced cell cycle arrest in the G0/G1 phase of *L. donovani* parasites. After treatment with different concentrations of synthesized Ag NPs (0, 12.5, 25 and 50 µg/mL, (a-d)) for 24 h, promastigotes were collected, washed with PBS and stained with PI, the DNA content was analysed by flow cytometry. (e) Graph showing % population in G0/G1, S and G2/M phase of treated parasites. (f) DNA fragmentation of *L. donovani* promastigotes treated with different concentrations of synthesized Ag NPs (12.5, 25 and 50 µg/mL). M represents DNA ladder, Lane 1 shows DNA from untreated cells while Lane 2, 3 and 4 represent DNA from synthesized Ag NPs treated cells. The data are presented as mean ± standard deviation of three independent experiments.

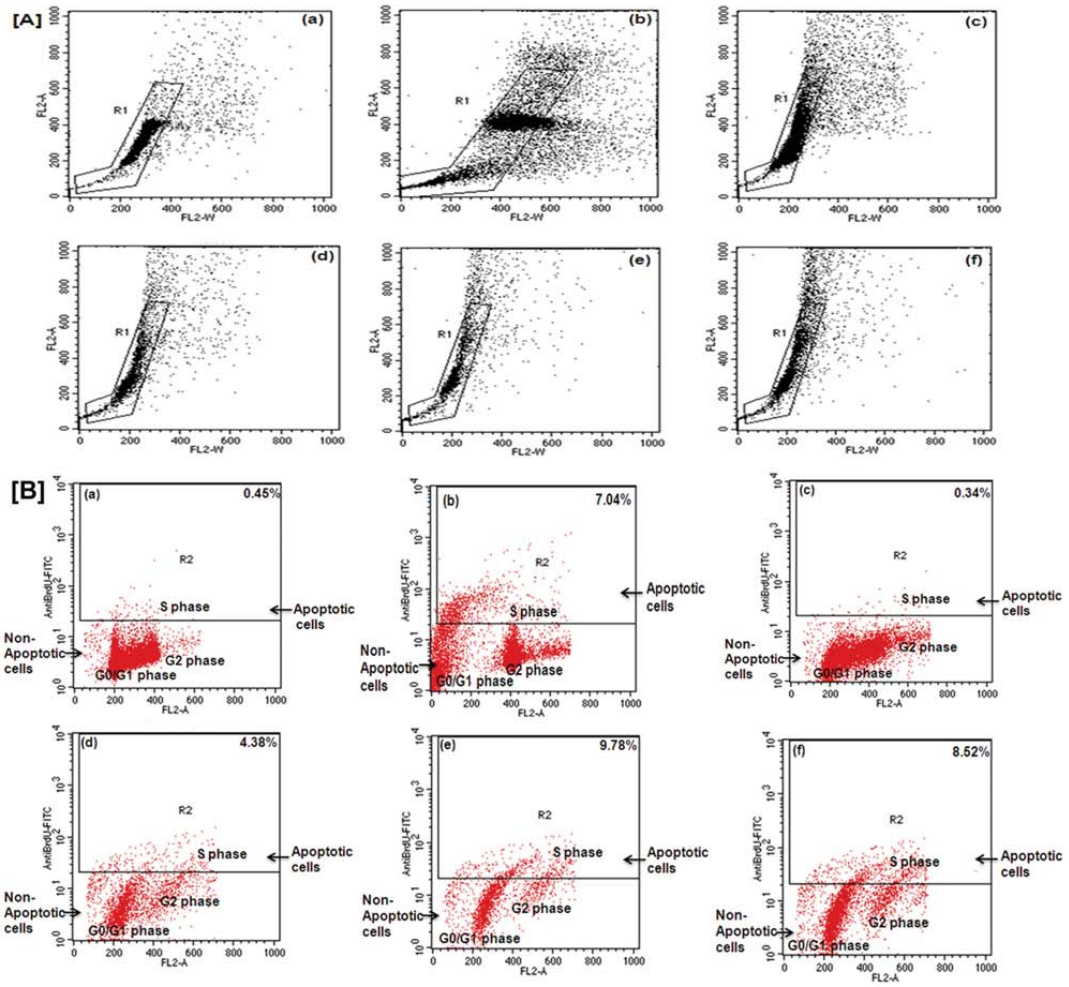

Figure 5. Synthesized Ag NPs-induced DNA fragmentation in promastigotes of *L. donovani* was analysed by TUNEL assay using flow cytometry. **[A]** Gating was done within the DNA Area on the Y-axis (FL2-A) and the DNA Width on the X-axis (FL2-W). **[B]** A gate was drawn around the non -clumped cells. Where the X axis depicts DNA (FL2 channel) and the Y axis depicts Anti-BrdU-FITC (FL1 channel). Increasing concentrations of synthesized Ag NPs showed the increase number of cells (R2) stained by anti-BrdU which have moved from non apoptotic population (G0/G1 and G2 phase) to the apoptotic population (S phase). (a) and (b) represent negative and positive control respectively (provided by kit) where (c), (d), (e) and (f) show promastigotes treated with different concentrations (0, 12.5, 25 and 50 µg/ml) of synthesized Ag NPs respectively.

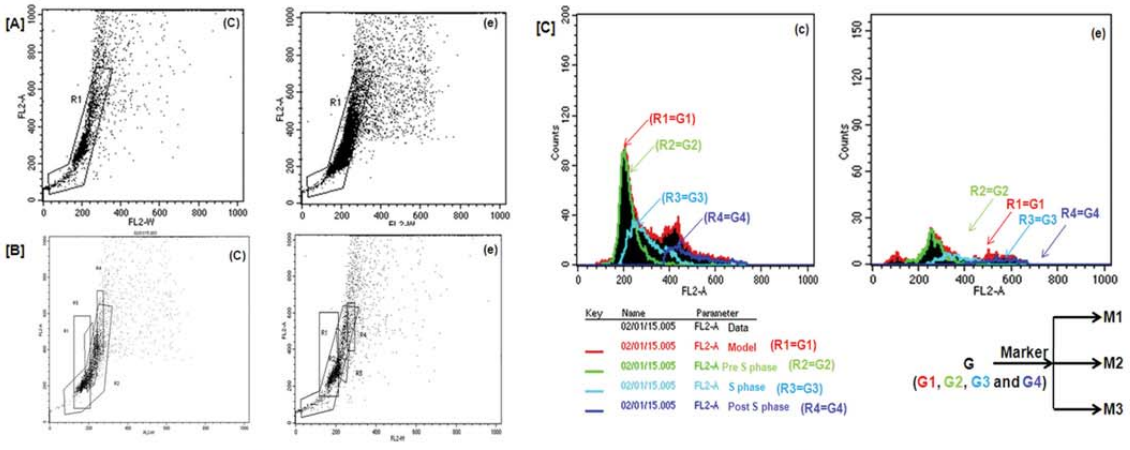

[D] (c)

Gate R1=G1

Marker	Left, Right	Events	% Gated	% Total	Geo Mean	CV	Peak Ch
All	0, 1023	10125	100.00	78.22	279.62	36.74	205
M1	145, 258	5002	49.40	38.64	208.08	11.27	205
M2	217, 398	4687	46.29	36.21	284.98	19.25	218
M3	353, 493	2583	25.51	19.95	413.87	8.57	431

Gate R2=G2

Marker	Left, Right	Events	% Gated	% Total	Geo Mean	CV	Peak Ch
All	0, 1023	5176	100.00	39.98	213.08	15.71	205
M1	145, 258	4614	89.14	35.64	206.11	10.89	205
M2	217, 398	2060	39.80	15.91	245.47	10.93	218
M3	353, 493	9	0.17	0.07	401.94	9.97	357

Gate R3=G3

Marker	Left, Right	Events	% Gated	% Total	Geo Mean	CV	Peak Ch
All	0, 1023	3448	100.00	26.64	281.67	20.62	233
M1	145, 258	1330	38.57	10.27	231.22	7.56	233
M2	217, 398	2956	85.73	22.84	283.37	16.70	233
M3	353, 493	571	16.56	4.41	389.68	6.25	380

Gate R4=G4

Marker	Left, Right	Events	% Gated	% Total	Geo Mean	CV	Peak Ch
All	0, 1023	1360	100.00	10.51	462.93	15.96	435
M1	145, 258	0	0.00	0.00	***	***	***
M2	217, 398	196	14.41	1.51	386.97	1.83	392
M3	353, 493	972	71.47	7.51	428.03	7.31	435

(e)

Gate R1=G1

Marker	Left, Right	Events	% Gated	% Total	CV	Median	Peak Ch
All	0, 1023	2028	100.00	47.11	39.70	280.00	245
M1	191, 310	1084	53.45	25.18	10.69	258.00	245
M2	290, 449	559	27.56	12.98	12.96	329.00	290
M3	416, 627	400	19.72	9.29	10.56	515.50	494

Gate R2=G2

Marker	Left, Right	Events	% Gated	% Total	CV	Median	Peak Ch
All	0, 1023	1162	100.00	26.99	15.19	257.00	245
M1	191, 310	999	85.97	23.21	10.62	255.00	245
M2	290, 449	238	20.48	5.53	6.49	307.00	290
M3	416, 627	0	0.00	0.00	***	***	***

Gate R3=G3

Marker	Left, Right	Events	% Gated	% Total	CV	Median	Peak Ch
All	0, 1023	456	100.00	10.59	16.06	349.00	303
M1	191, 310	107	23.46	2.49	5.79	290.00	303
M2	290, 449	369	80.92	8.57	12.09	352.00	303
M3	416, 627	83	18.20	1.93	4.26	444.00	433

Gate R4=G4

Marker	Left, Right	Events	% Gated	% Total	CV	Median	Peak Ch
All	0, 1023	178	100.00	4.13	10.95	541.00	526
M1	191, 310	0	0.00	0.00	***	***	***
M2	290, 449	11	6.18	0.26	3.65	439.00	439
M3	416, 627	158	88.76	3.67	9.43	533.00	526

Table 1. Comparison of estimates of S phase by Flow Cytometry:

Marker	Pre S phase (%) G2	S phase (%) G3	Post S phase (%) G4
M1 (c)	35.64	10.27	0.00
M1 (e)	23.21	2.49	0.00
M2 (c)	15.91	22.84	1.51
M2 (e)	5.53	8.57	0.26
M3 (c)	0.07	4.41	7.51
M3 (e)	0.00	1.93	3.67

Figure 6. The length of S phase varies according to the percentage of DNA content in untreated and treated promastigotes of *L. donovani*. By using the dual parameter display method **[A]** A gate was drawn around the non -clumped cells (R1) and **[B]** R1 gated cells were divided into three sub gates which were R2, R3 and R4. **[C]** We further applied markers (M1 ,M2 and M3) on the sub gates R2, R3 and R4 to denote G2, G3 and G4 ~ depicting pre S phase, S phase and post S phase respectively. **[D]** Show the statistics analysis of sub gated cells of *L. donovani*. **(Table. 1)** S phase halt (in term of percentage of DNA content) was prominent in cells treated with 25 µg/ml of synthesized Ag NPs as compared to untreated cells. Where (c) and (e) denote untreated parasites and parasites treated with 25 µg/ml of synthesized Ag NPs respectively.

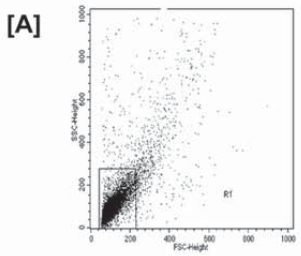

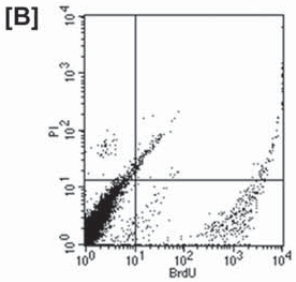

Quadrant Statistics

File: 01/01/15.001
Acquisition Date: 01-Jan-15
Gated Events: 10000
X Parameter: BrdU (Log)
Quad Location: 10, 13

Log Data Units: Linear Values
Gate: No Gate
Total Events: 10000
Y Parameter: PI (Log)

Quad	Events	% Gated	% Total
UL	147	1.47	1.47
UR	201	2.01	2.01
LL	9292	92.92	92.92
LR	360	3.60	3.60

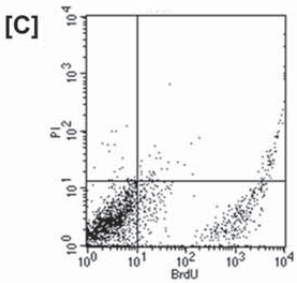

Quadrant Statistics

File: 01/01/15.006
Acquisition Date: 01-Jan-15
Gated Events: 2070
X Parameter: BrdU (Log)
Quad Location: 10, 13

Log Data Units: Linear Values
Gate: No Gate
Total Events: 2070
Y Parameter: PI (Log)

Quad	Events	% Gated	% Total
UL	24	1.16	1.16
UR	90	4.35	4.35
LL	1522	73.53	73.53
LR	434	20.97	20.97

Figure 7. The length of S phase in term of time duration was determined by double labeling method: **[A]** Gating was done using forward scatter (FSC) versus side scatter (SSC). **[B and C]** Fluorescence was measured in the log mode using CellQuest Pro software (BD Biosciences, CA). Where x-axis depicts BrdU and y-axis depicts PI. **[B]** Represents the histogram of untreated promastigotes and **[C]** represents the histogram of treated (with 25 µg/ml of synthesized Ag NPs) promastigotes respectively.

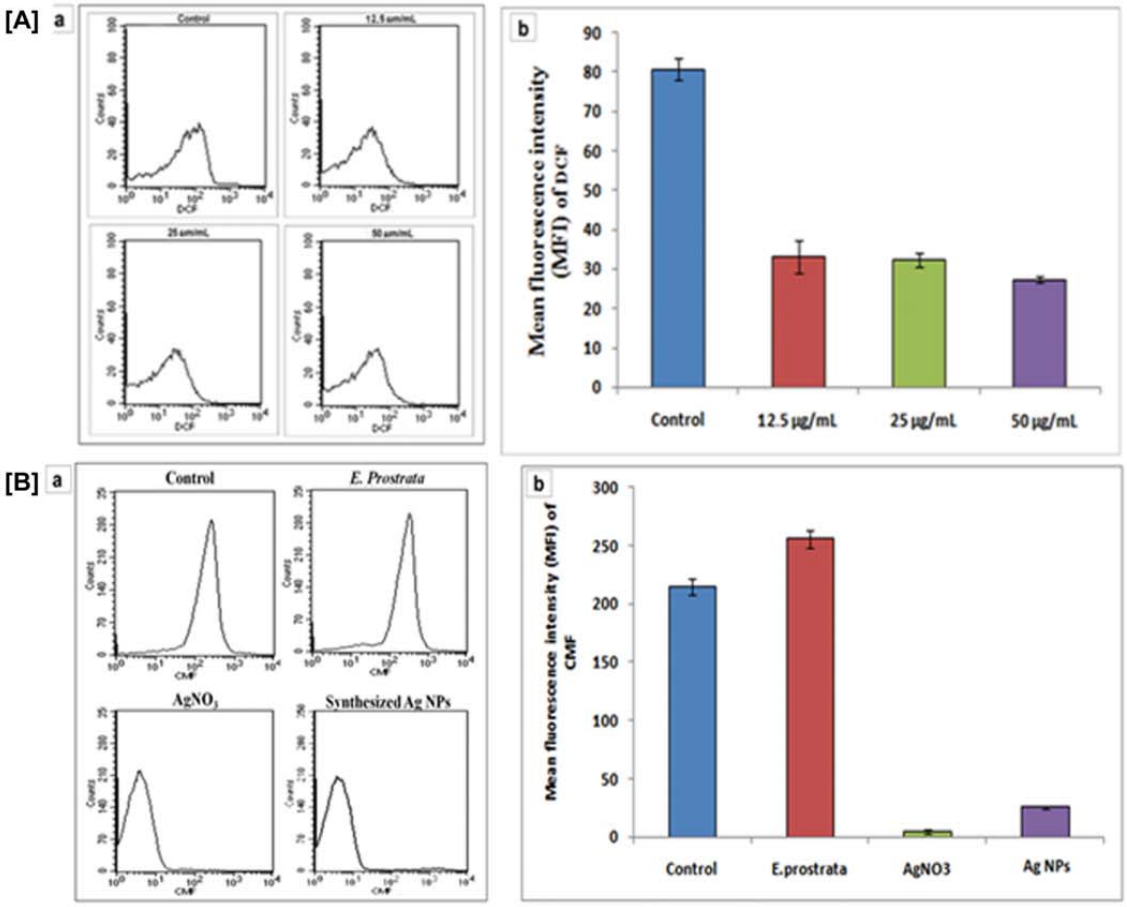

Figure 8. [A] ROS generation was measured using the fluorescent dye 2,7 dichlorodihydrofluorescein diacetate after treatment with (a) different concentrations (12.5, 25 and 50 µg/ml) of synthesized Ag NPs for 24 h and its fluorescence was measured using a flow cytometer. (b) Graph shows mean fluorescence intensity of DCF in control and synthesized Ag NPs treated cells at 24 h. The data are presented as mean ± standard deviation of three independent experiments. **[B]** Intracellular level of the glutathione (GSH) in *L. donovani* promastigotes treated with *E.prostrata*, $AgNO_3$solution and synthesized Ag NPs. (b) Graph shows mean fluorescence intensity of CMF (GSH sensitive probe) in control, *E. prostrata*, $AgNO_3$ and synthesized Ag NPs treated cells at 24 h. The data are presented as mean ± standard deviation of three independent experiments.

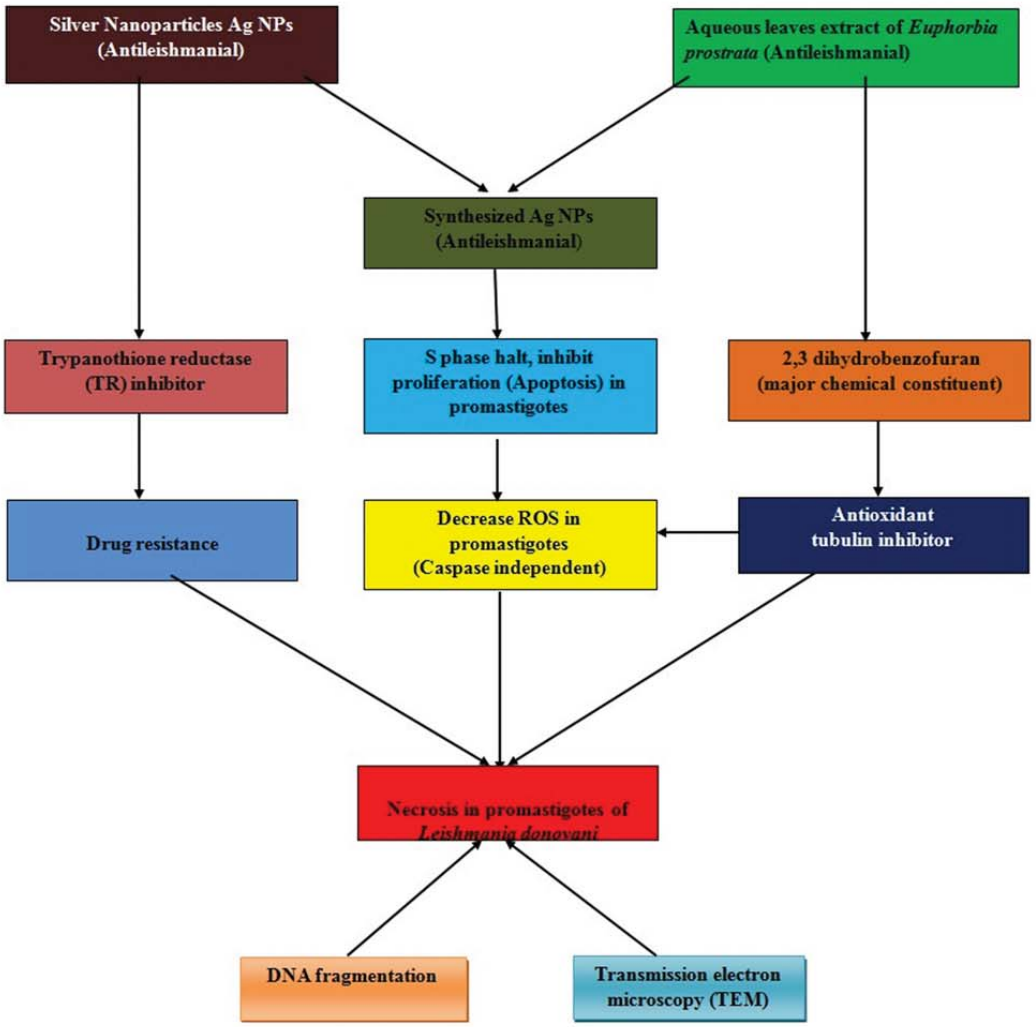

Figure 9. Schematic diagram of proposed mechanism of synthesized Ag NPs induced cell death in *L. donovani* promastigotes. Synthesized Ag NPs inhibit promastigotes proliferation and induced caspase independent cell death which is largely due to necrosis. Cell death in *L. donovani* promastigotes is accompanied by decreased level of intracellular non-protein thiols and reactive oxygen species.